Astron Astrophys Rev (2023)31:2
https://doi.org/10.1007/s00159-023-00147-4

REVIEW ARTICLE

Growth of cosmic structure

Dragan Huterer[1]

Received: 7 December 2022 / Accepted: 5 June 2023

Abstract

We review one of the most fruitful areas in cosmology today that bridge theory and data—the temporal growth of large-scale structure. We go over the growth's physical foundations, and derive its behavior in simple cosmological models. While doing so, we explain how measurements of growth can be used to understand theory. We then review how some of the most mature cosmological probes—galaxy clustering, gravitational lensing, the abundance of clusters of galaxies, cosmic velocities, and cosmic microwave background—can be used to probe the growth of structure. We report the current constraints on growth, which are summarized as measurements of the parameter combination $f\sigma_8$ as a function of redshift, or else as the mass fluctuation amplitude parameter S_8. We finally illustrate several statistical approaches, ranging from the "growth index" parameterization to more general comparisons of growth and geometry, that can sharply test the standard cosmological model and indicate the presence of modifications to general relativity.

Keywords Cosmology · Large-scale structure · Dark energy · Modified gravity

Contents

✉ Dragan Huterer
huterer@umich.edu

[1] Department of Physics and Leinweber Center for Theoretical Physics, University of Michigan, 450 Church St, Ann Arbor, MI 48103, USA

Published online: 30 June 2023

1 Introduction

In the standard cosmological model, the seeds of structure laid out by inflation were amplified by the influence of gravity. The density perturbation is defined as

$$\delta(\mathbf{x}, t) \equiv \frac{\delta\rho(\mathbf{x}, t)}{\bar{\rho}}, \tag{1}$$

where ρ is density in matter, and $\mathbf{x}$ and t denote space and time coordinates, respectively. Density perturbations are seeded by inflation, start out with an amplitude $\delta \simeq 10^{-5}$, and are subsequently amplified by gravity over the ensuing billions of years in a way that is described by Eq. (2) below. The general fact that structure grows over time is a very well-established feature of the hot big-bang cosmological model. The growth of structure can be measured through observations of positions and motions of galaxies as a function of cosmic time, and by comparing the inferred overdensities to the initial conditions, $\delta \sim 10^{-5}$, that can be observed in the temperature anisotropies of the cosmic microwave background (CMB).

A cosmological model predicts the temporal growth of structure. Such a prediction is a key ingredient in theoretical calculations of the various observable quantities that can be experimentally measured. For example, weak-lensing shear integrates the power spectrum of structure along the line of sight (as we discuss in Sect. 3.2), which is in turn is determined by the growth of structure. As another example, the amplitude of galaxies' peculiar velocities and the spatial correlations of galaxy positions are both largely determined by the growth of structure. In all of these examples, a larger rate of growth corresponds to a larger signal (assuming fixed initial conditions). Turning the argument around, measurements of the large-scale structure and inference of its statistical properties inform us about the growth of structure. In turn, constraints on the growth of structure help pin down the parameters of the cosmological model, and are especially sensitive to the properties of dark energy.

Over the past two decades, the advent of massive new datasets from large-scale structure has brought into focus the importance of the growth of structure. This is principally because growth is a sensitive probe of both dark energy and modified gravity, as hence its measurements can distinguish between the two. Specifically, in the context of general relativity, growth is mathematically related to the geometrical

measures such as distances. Specifically, growth of structure affects the expansion rate given by the Hubble parameter H, which in turn affects distances (as H enters the distance-redshift relation). Therefore, growth is directly related to the geometrical quantities in the universe. However, this relation between growth and geometry assumes Einstein's general relativity, and is generally broken (or modified) when gravity itself is modified. Comparing growth to geometry, thus, enables stringent tests of modified gravity.

The purpose of this review is to present a rather high-level review of the growth of structure, aimed at a non-expert astrophysicist. Our main goal is to lay out the theoretical foundations for basic studies of growth. We also wish to illustrate, at a basic yet quantitative level, how growth enters the various cosmological probes, and how they can be used to measure growth. Finally, we review some of the most promising strategies to use growth to better understand dark energy and modified gravity. This review focuses on the big-picture foundations of the subject and the cosmological utility of the growth of structure (as well as current constraints), and updates and complements the previous major reviews of the subject (Weinberg et al. 2013; Huterer et al. 2015) which focused on future surveys and expected systematic errors in the associated cosmological probes.

This review is organized as follows. In Sect. 2, we discuss the theoretical background useful for understanding growth of structure. In Sect. 3, we review the observations that are sensitive to growth, and compile recent constraints on the growth of structure. In Sect. 4, we discuss ways in which the growth of structure can be used to probe dark energy and general relativity. We conclude in Sect. 5.

2 Theoretical background

Here, we outline the theoretical predictions for the growth of cosmic structure. We start with density perturbations, introduce the (linear) growth of structure, derive an equation that governs its evolution in time, and study its solutions.

2.1 Temporal evolution of linear density perturbations

In our theoretical treatment, we will specialize in linear theory, and assume small fluctuations, with $|\delta| \ll 1$. To make even better progress, we expand the overdensity in Fourier basis. We do so because it turns out that each Fourier mode $\delta_{\mathbf{k}}$ evolves independently (assuming linear perturbations and standard general relativity). Following a standard, non-relativistic, perturbation-theory analysis that combines the continuity, Euler, and Poisson equations, one arrives at (e.g., Mo et al. 2010; Huterer 2023)

$$\frac{\partial^2 \delta_{\mathbf{k}}}{\partial t^2} + 2\frac{\dot{a}}{a}\frac{\partial \delta_{\mathbf{k}}}{\partial t} = \left(4\pi G\rho_{\mathrm{M}} - \frac{k^2 c_s^2}{a^2}\right)\delta_{\mathrm{k}} - \frac{2}{3}\frac{T}{a^2}k^2 S_{\mathbf{k}}, \tag{2}$$

where T is temperature, a is the scale factor, c_s is the speed of sound, and ρ_{M} is the mean matter density; all of these quantities depend on cosmic time t. Further, $\delta_{\mathbf{k}}$ is the mode in the Fourier expansion of the overdensity field at some wavenumber $\mathbf{k}$

$$\delta_{\mathbf{k}}(t) = \frac{1}{\sqrt{V}} \int \delta(\mathbf{r}, t) e^{-i\mathbf{k}\cdot\mathbf{r}} d^3\mathbf{r}. \tag{3}$$

Here, V is the volume of the larger region over which the perturbations are assumed to be periodic (note that $\mathbf{k}$ and $\mathbf{r}$ are both comoving quantities). Similarly, $S_{\mathbf{k}}$ is the Fourier mode of entropy perturbations.

We further specialize in isentropic initial conditions where there is no fluctuation in entropy in the initial conditions, so that $S_{\mathbf{k}} \propto \nabla S = 0$. [Confusingly, these fluctuations are most often called adiabatic initial conditions, which strictly speaking implies $\dot{S} = 0$, not $\nabla S = 0$; we henceforth adopt this imprecise but popular nomenclature.] In the presence of adiabatic initial conditions, fluctuations in various components (matter, radiation, neutrinos, etc.) are proportional to each other, and the overall curvature fluctuation is nonzero. This is the kind of initial condition that inflation typically predicts, and that current data favor. Finally, we specialize in fluctuations on scales larger than the Jeans scale, so $k \ll k_{\rm Jeans} \equiv \sqrt{4\pi G \rho_{\rm M}}(a/c_s)$. This is a reasonable assumption since, after recombination, the Jeans scale corresponds to mass of order $10^5\, M_\odot$, which is much smaller than the structures that we will be interested in which are roughly mass of a galaxy or larger, so $\gtrsim 10^{12}\, M_\odot$. In this regime, we can drop the term that is proportional to k^2. With all that, Eq. (2) simplifies to

$$\ddot{\delta} + 2H\dot{\delta} - 4\pi G \rho_{\rm M} \delta = 0, \tag{4}$$

where $H \equiv \dot{a}/a$ is the Hubble parameter. Notice that we have dropped the subscript $_{\mathbf{k}}$ in the overdensity, as there is no more wavenumber dependence in this equation.

Equation (4) describes the evolution of the density perturbations on scales $0.001\, h\,{\rm Mpc}^{-1} \lesssim k \lesssim 0.1\, h\,{\rm Mpc}^{-1}$, which is where the most usable observational data reside. [On scales larger than about $0.001\, h\,{\rm Mpc}^{-1}$ there are additional general-relativistic corrections and may anyway difficult to probe, while scales smaller than about $0.1\, h\,{\rm Mpc}^{-1}$ lie in the non-linear regime; see the bullet points below for further discussion.] This is a second-order ordinary differential equation for the matter overdensity δ. We will solve it below to get solutions for the linear growth of structure in simple cosmological models.

Let us first review the assumptions that were assumed in deriving Eq. (4):

- General theory of relativity;
- Adiabatic initial conditions;
- Sub-horizon scales (i.e., relativistic effects are ignored); $k \gg H_0$;
- Spatial scales above the Jeans length ($k \ll k_J$);
- Linear theory ($\delta \ll 1$), which corresponds roughly to scales $k \lesssim 0.1\, h\,{\rm Mpc}^{-1}$ today.

The breakdown of any of these assumptions could lead to the invalidation of Eq. (4), which would be manifested as a difference between the predicted and observed growth. The growth of structure can of course be theoretically predicted when either

one of the assumptions above is relaxed, but those predictions tend to be more detail dependent, have functional or numerical forms that are necessarily more complicated, and are also in the regimes where the comparison to data is more difficult (see the discussion in the bulleted list just below). Therefore, we will largely stick to studying the growth as given in Eq. (4), with the assumptions given in the bullet points above. Before proceeding, however, we wish to comment further about a few of these assumptions and situations in which relaxing them may be relevant:

- **Beyond general relativity:** Our assumption of Einstein's general relativity in deriving Eq. (4) deserves particular attention, as modified-gravity theories generically lead to the scale dependence of $\delta(t)$. Observing this scale dependence, and ruling out the systematic errors as the cause, would present striking evidence for the presence of modified gravity. There has been growing interest in trying to constrain the scale-dependent predictions of the growth of structure with current and future surveys (Zhao et al. 2009b, a; Daniel and Linder 2010; Zhao et al. 2010; Song et al. 2011; Silvestri et al. 2013).
- **Near-horizon scale:** Equation (4) is modified on scales approaching the Hubble distance, $k \simeq H_0 \simeq 10^{-3}\, h\,\mathrm{Mpc}^{-1}$. This is due to relativistic effects which can be precisely quantified (Yoo et al. 2009; Yoo 2010; Challinor and Lewis 2011; Jeong et al. 2012; Bonvin 2014; Tansella et al. 2018; Grimm et al. 2020). Detecting these relativistic effects would be a very interesting test of the standard cosmological model, is challenging given that they appear on very large scales, but may nevertheless be possible with forthcoming large-scale structure surveys (Maartens et al. 2013; Alonso et al. 2015; Alonso and Ferreira 2015; Fonseca et al. 2015; Abramo and Bertacca 2017; Barreira 2022).
- **Beyond linear theory:** this assumption is the most "ready" to be relaxed, as a large portion of current observations lies in the quasi-linear or fully non-linear regime. In addition to pure gravitational non-linearities which can be reasonably accurately modeled using a combination of numerical and analytic tools, these scales are also affected by effects of baryons which affect the clustering on scales of a few megaparsecs and below. Current surveys [e.g., KiDS (Asgari 2021), DES (Abbott et al. 2023a), and HSC (Hikage 2019)] explicitly throw out scales that are strongly affected by baryons, but even then some information comes from quasi-linear regime where Eq. (4) does not hold. This puts premium on our ability to model the growth of structure in this regime with a combination of numerical and analytic tools. Such predictions are available in ΛCDM (cosmological model with vacuum energy and cold dark matter) (Hamilton et al. 1991; Peacock and Dodds 1996; Smith et al. 2003; Heitmann et al. 2009; Takahashi et al. 2012; Heitmann et al. 2014; Mead et al. 2015; Garrison et al. 2018; Bird et al. 2018; DeRose et al. 2019; Mead et al. 2020), but more recent work has extended this to dark energy models with the equation of state parameterized by (w_0, w_a) (Linder and Jenkins 2003; Francis et al. 2007; Casarini et al. 2016; Lawrence et al. 2017; Knabenhans et al. 2021), as well as modified-gravity models (Stabenau and Jain 2006; Laszlo and Bean 2008; Oyaizu et al. 2008; Baldi et al. 2010; Koyama et al. 2009;

Schmidt 2009; Chan and Scoccimarro 2009; Zhao et al. 2011; Li et al. 2013; Barreira et al. 2014; Winther 2015; Bose et al. 2017).

2.2 Growth in simple cosmological models

The growth Eq. (4) can of course be solved numerically for an arbitrary cosmological model—the input required is the scaling of the Hubble parameter with time, $H(t)$, and that of the matter density, $\rho_{\rm M}(t)$. However, it is instructive to derive scalings in single-component universes, where the expansion is dominated by a single component—matter, radiation, or dark energy.

Let us start with the radiation-dominated case. Then, $a \propto t^{1/2}$, so that $H(t) \equiv \dot{a}/a \propto 1/(2t)$. Also, note that the last term in Eq. (4) is negligible because the Hubble parameter is dominated by the radiation and not matter density, so that $4\pi G\rho_{\rm M} \ll H^2$. Therefore, we need to solve the equation $\ddot{\delta} + 2H\dot{\delta} = 0$, with $H = 1/(2t)$. Its solution is

$$\delta(t) = A_1 + A_2 \ln t \qquad \text{(radiation dominated)}, \tag{5}$$

where A_1 and A_2 are some constants. Thus, in the radiation-dominated regime, the fluctuations grow only very slowly—logarithmically with time.

In the flat, matter-dominated (Einstein–de Sitter) case, $a \propto t^{2/3}$ so that $H(t) \equiv \dot{a}/a \propto 2/(3t)$, while the Hubble parameter is dominated by matter density, so that $4\pi G\rho_{\rm M} = (3/2)H^2$. Let us assume that $\delta(t) \propto t^n$; then the growth equation simplifies to $n(n-1) + \frac{4}{3}n - \frac{2}{3} = 0$. Its solutions are easy to obtain: $n = +2/3$ and -1. Hence

$$\delta(t) = B_1 t^{2/3} + B_2 t^{-1} \qquad \text{(matter dominated)}, \tag{6}$$

where B_1 and B_2 are some constants. Since $a(t) \propto t^{2/3}$ in the matter-dominated era, the growing mode of the perturbations grows proportionally to the scale factor, $\delta(t) \propto a(t) \propto t^{2/3}$. This scaling is of the utmost importance, as the universe spends of order 10 billion years in the matter-dominated era—from the matter-radiation equality 50,000 years after the Big Bang, to the onset of dark energy a few billion years ago. During that time, structures in the universe grow appreciably, all thanks to the $\delta \propto a$ scaling.

Finally, in the dark-energy-dominated era, which will presumably take place in the future when dark energy dominates completely, the scale factor grows exponentially,[1] $a \propto e^{Ht}$, so that $H(t) \equiv H_\Lambda = \text{const}$. [Here we are representing dark energy by a specific model, that of the cosmological constant Λ, which mathematically represents vacuum energy which has a constant energy density across cosmic time.] Also, note that the last term in Eq. (4) is negligible since the matter density is negligible relative to vacuum energy in H. Therefore, we need to solve the equation $\ddot{\delta} + 2H_\Lambda\dot{\delta} = 0$ whose solution is

[1] The same happens during inflation, when the universe is completely vacuum-energy dominated.

$$\delta(t) = C_1 + C_2 e^{-2H_\Lambda t} \simeq \text{const} \qquad \text{(Lambda dominated)}, \tag{7}$$

where C_1 and C_2 are some constants, and where the exponentially decaying term becomes negligible quickly. Therefore, density perturbations do not grow at all in a Lambda-dominated universe. We are all witnesses to this effect today, as our universe with 70% dark-energy and 30% matter displays severely suppressed structure formation (relative to the matter-only scenario), something that is readily observed in the cosmological data that probe $z \lesssim 1$ using tests that we describe in Sect. 3.

Summarizing, the temporal evolution of linear density perturbations in simple, single-component cosmological models is:

$$\delta(a) \propto \begin{cases} t^{2/3} \propto a & \text{(matter dominated)} \\ \ln(t) \propto \ln(a) & \text{(radiation dominated)} \\ \text{const} & \text{(Lambda dominated)}\,, \end{cases} \tag{8}$$

where a is the scale factor.

2.3 Dimensionless linear growth function

It is useful to cast Eq. (4) in a dimensionless form. Let us introduce the *linear growth function*

$$D(a) = \frac{\delta(a)}{\delta(1)}, \tag{9}$$

where D at the present time is unity, $D(1) = 1$. The original equation determining the linear growth of structure, Eq. (4), can now be set in a dimensionless form as

$$2\frac{d^2 g}{d\ln a^2} + [5 - 3w(a)\Omega_{\rm DE}(a)]\frac{dg}{d\ln a} + 3[1 - w(a)]\Omega_{\rm DE}(a) g = 0, \tag{10}$$

where $g \equiv g(a)$ is the *growth suppression factor*—that is, growth relative to that in Einstein-de Sitter ($\Omega_{\rm M} = 1$) universe. The linear growth suppression factor g is related to the growth factor D implicitly via

$$D(a) \equiv \frac{a g(a)}{g(1)}. \tag{11}$$

Note that the linear growth function depends on the Hubble parameter $H(a)$, as well as the matter density $\Omega_{\rm M}$. Thus the linear growth function depends on basic cosmological parameters; in the flat ΛCDM model for example, $D = D(a, \Omega_{\rm M})$, and same for g. In particular, the growth function does not depend on wavenumber k. [This is no longer true in modified-gravity models as explained above, but also in models with massive neutrinos, which introduce a mild scale-dependence to the linear growth function (Lesgourgues and Pastor 2006).]

Figure 1 shows the temporal evolution of $D(z)$ and $g(z)$ in the standard cosmological ΛCDM model with $\Omega_{\rm M} = 1 - \Omega_\Lambda = 0.3$ (in what follows, we will

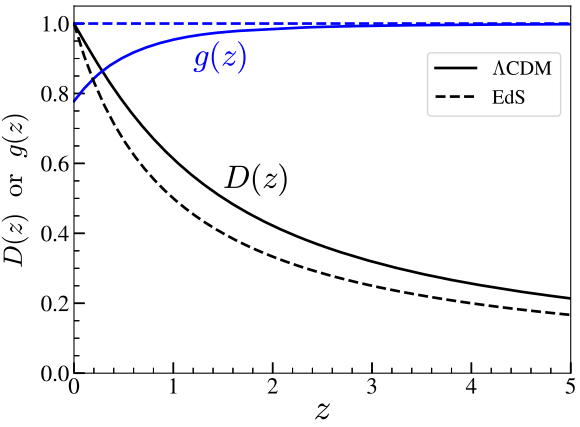

Fig. 1 Illustration of the linear growth function $D(z)$ and the growth suppression factor $g(z)$, as a function of redshift z, in the standard flat ΛCDM cosmological model. For comparison, we also show the results in the flat model with dark matter only ($\Omega_{\rm M} = 1$), the Einstein–de Sitter (EdS) model. Either $D(z)$ or $g(z)$ fully describes the linear growth of fluctuations; see text for details

frequently switch between redshift z and scale factor $a = 1/(1+z)$). For comparison, we also show the results in the flat model with dark matter only ($\Omega_{\rm M} = 1$), the Einstein–de Sitter (EdS) model. In ΛCDM, the onset of dark energy at late times ($z \lesssim 1$) causes these functions to deviate from their EdS behavior ($D(a) = a$ or $D(z) = 1/(1+z)$, and $g(z) = 1$). The late-time decrease in either $g(z)$ or $D(z)$ fully specifies the suppression in the growth of structure (in linear theory) due to dark energy. In our fiducial flat ΛCDM cosmological model with $\Omega_{\rm M} = 1 - \Omega_{\rm DE} = 0.3$, the present-day value of the suppression factor is $g(z=0) \simeq 0.78$.

Linear growth function enters the linear matter power spectrum in a straightforward way. The matter power spectrum, $P(k)$, quantifies the amount of structure—the power—at each wavenumber k. The power spectrum is defined in terms of the two-point correlation function of Fourier-space overdensity $\delta_{\mathbf{k}}$ as

$$\langle \delta_{\mathbf{k}}\, \delta^*_{\mathbf{k}'} \rangle = (2\pi)^3\, \delta^{(3)}(\mathbf{k} - \mathbf{k}')\, P(k,a), \tag{12}$$

where the angular brackets denote ensemble average, and $\delta^{(3)}$ is the Dirac delta function. Note that the power spectrum depends only on the magnitude of the wavenumber, $k = |\mathbf{k}|$, due to the assumptions of homogeneity and isotropy. Because $\delta_{\mathbf{k}}(a) \propto D(a)$ by definition, the dependence of the linear matter power spectrum on the linear growth is simple enough,

$$P(k,a) \propto D(a)^2 \propto [a g(a)]^2, \tag{13}$$

or, entirely equivalently, $P(k,z) \propto D(z)^2$. Therefore, a simple observation of how galaxy clustering scales with redshift is sensitive to the growth of structure. This is, however, only one way to probe the growth, as cosmological observations are sensitive to its different aspects, only some of which are captured in Eq. (13). We now cover this in more detail.

3 Connection to observations

There are several ways in which one can measure the growth of structure through cosmic time. Measuring galaxy clustering in redshift effectively measures $P(k, z)$ in (typically) several redshift bins, thus probing growth. Additionally, one can map out the cosmic shear pattern, measuring correlations of shapes of distant galaxies which is sensitive to the distribution of mass along the line of sight and thus the growth of structure. Cross-correlating galaxy clustering and cosmic-shear signal is another method that can provide additional information on growth. A rather different approach entails measuring the space density of clusters of galaxies; their density as a function of mass and redshift—the mass function—depends on the linear growth function $D(z)$. Finally, one can measure the correlation of galaxy velocities as it too is sensitive to growth. We now discuss these cosmological probes, and how growth enters them.

3.1 Galaxy clustering

Because galaxy clustering is one of the principal cosmological probes, its measurements provide the principal way to isolate and constrain the growth of cosmic structure. Measurements of galaxy clustering constrain the power spectrum $P(k, z)$ or, equivalently, the two-point correlation function $\xi(r, z)$, over a range of scales and in several redshift bins. It is the dependence on redshift z that informs us about the temporal growth of cosmic structure.

We now quantify the dependence of clustering on growth. The linear ($|\delta| \ll 1$) dimensionless matter power spectrum $\Delta^2(k, z)$ can be expressed in terms of $P(k)$ as

$$\begin{aligned}\Delta^2(k,z) &\equiv \frac{k^3 P(k,z)}{2\pi^2} \\ &= A_s \, \frac{4}{25}\frac{1}{\Omega_{\rm M}^2}\left(\frac{k}{k_{\rm piv}}\right)^{n_s-1}\left(\frac{k}{H_0}\right)^4\left(\frac{g(z)}{1+z}\right)^2 T^2(k),\end{aligned} \tag{14}$$

where we expressed the temporal dependence in terms of redshift z. Here, A_s is the normalization of the power spectrum (for the fiducial cosmology, $A_s \simeq 2.1 \times 10^{-9}$), n_s is the spectral index, $k_{\rm piv}$ is the "pivot" around[2] which $\Delta^2(k)$ varies as a power law in wavenumber, the combination $ag(a) \equiv g(z)/(1+z) \propto D(z)$ determines the linear growth of perturbations, and $T(k)$ is the linear transfer function which mainly encodes the change in the shape of the power spectrum around the scale corresponding to horizon size at matter-radiation equality.

Dependence of the linear matter power spectrum on the (linear) growth in Eq. (14) is simple enough, $P(k, z) \propto g(z)^2 \propto D(z)^2$. However, in practice there are two complications:

[2] Typically tajen to be $k_{\rm piv} = 0.05\,{\rm Mpc}^{-1}$, which is close to the wavenumber at which the primordial power is best constrained.

- First, we can measure the power spectrum of galaxies and not dark-matter particles. Traditionally, the relationship between the galaxy overdensity $(\delta\rho)_g/\rho_g$ and the matter overdensity $\delta\rho/\rho$ is given by the so-called galaxy bias term, $b \equiv [(\delta\rho)_g/\rho_g]/[(\delta\rho)/\rho]$. The relationship between the galaxy power spectrum and the matter power spectrum is consequently

$$P_{gg}(k,z) = b^2(k,z)P(k,z), \tag{15}$$

  where $b(k, z)$ is galaxy bias which depends on the wavenumber in a way that may be difficult to predict theoretically. Further, galaxy bias depends on the galaxy type and, worse, on the galaxy formation history (often termed "assembly bias"), and thus typically needs to be measured directly from the data. Even on linear scales, where galaxy bias is expected to be scale-independent (i.e., constant in wavenumber k), its time dependence is a priori unknown. This time dependence of the bias is unfortunately degenerate with that of the growth of structure, and breaking this degeneracy requires either independent prior information on the bias or else combination of galaxy clustering with other cosmological measurements.[3]
- The second complication is that typical clustering measurements are made partly in the quasi-linear and non-linear regime, corresponding roughly to scales $r \lesssim 10\,h^{-1}\mathrm{Mpc}$ (or $k \gtrsim 0.1\,h\,\mathrm{Mpc}^{-1}$) at $z = 0$. Non-linear corrections to the matter power spectrum also depend on scale, while additional scale dependence in galaxy clustering is brought about by baryonic effects, as well as the dependence of galaxy bias $b(k, z)$ on scale. The resulting effects on the galaxy power spectrum are not theoretically tractable and must be calibrated with N-body simulations—ideally hydrodynamical simulations which contain both the baryon and the dark matter particles.

Traditionally, cosmological constraints from galaxy clustering have been quoted in terms of constraints on the amplitude of mass fluctuations $\sigma(z, R)$. This quantity effectively averages the matter power spectrum evaluated at some redshift z over a spherical region of comoving radius R. Mathematically,

$$\sigma^2(z,R) = \int_0^\infty \Delta^2(k,z)\left(\frac{3j_1(kR)}{kR}\right)^2 d\ln k, \tag{16}$$

where $\Delta^2(z,k)$ is the dimensionless power spectrum from Eq. (14). The galaxy-clustering constraints are typically converted to those on the amplitude of mass fluctuations evaluated at $z = 0$ and $R = 8\,h^{-1}\mathrm{Mpc}$—hence, we often make use of the quantity $\sigma_8 \equiv \sigma(z = 0, R = 8\,h^{-1}\mathrm{Mpc})$.

[3] There is no way to break this degeneracy between the time dependence of bias and growth with galaxy clustering alone. However, as we discuss in Sect. 3.2, one can use weak gravitational lensing (which altogether avoids galaxy bias), as well as galaxy–galaxy lensing (proportional to bias, rather than bias squared), to break this degeneracy and isolate the growth of structure. Alternatively, simultaneous measurements of the power spectrum and other statistics of galaxy clustering (e.g., the three-point correlation function, or the bispectrum) can help separately constrain galaxy bias and the growth of structure.

Galaxy clustering is a mature cosmological probe, as its first measurements date to 1960s and 70s. It is also reasonably easily accessible—one only needs to measure the galaxy positions in order to calculate the correlation function. Ideally galaxy redshifts are available, in which case the full 3D power spectrum can be computed, otherwise one needs to determine the redshifts approximately using photometric information from galaxies (for a review of photometric redshifts, see Newman and Gruen 2022). However, the comparison of galaxy clustering with theoretical predictions is seriously challenged by the presence of galaxy bias, as we discussed above. This is where weak gravitational lensing comes in as a very powerful complement; we discuss this next.

3.2 Cosmic shear

Weak gravitational lensing—subtle distortions in galaxy shapes due to the intervening large-scale structure—is a very powerful probe of the growth of cosmic structure. Weak lensing is sensitive to the presence and distribution of mass along the line of sight, between the observer and source galaxies. This method, proposed in the 1960 s and first detected in the year 2000, is now a standard-bearer for the probes of large-scale structure. Weak lensing also goes under the name *cosmic shear* as one statistically measures the amount of shearing of the observed shape of galaxies caused by photon deflections, which in turn informs about the projected mass along the line of sight. See Bartelmann and Schneider (2001) and Hoekstra and Jain (2008) for reviews of weak lensing / cosmic shear.

The principal feature of cosmic shear is the absence of galaxy bias. Even though measuring galaxy shapes (for cosmic shear) is more challenging than measuring galaxy positions (for galaxy clustering), this absence of possible degeneracies between the bias and the growth of structure makes cosmic shear a premier cosmological probe.

A key quantity in cosmic shear is the convergence κ, which is defined at every point on the sky and is proportional to the projected matter density between the observer and the source galaxy. Specifically, convergence for a single lens and single source galaxy is given by

$$\kappa = \frac{d_{\rm L} d_{\rm LS}}{d_{\rm S}} \int_0^{\chi_{\rm S}} \nabla^2 \Phi \, d\chi, \tag{17}$$

where $d_{\rm L}$, $d_{\rm S}$, and $d_{\rm LS}$ are, respectively, the distance from the observer to the lens and to the source, and the distance between the lens and the source. Here, d is the angular diameter distance which is related to the comoving distance r via $d(z) = r(z)/(1+z)$, while χ is the coordinate distance and is related to the comoving distance via standard relations involving a sine or a sinh (Huterer 2023); in a flat universe, $r = \chi$. Further, Φ is the three-dimensional gravitational potential that gets integrated along the line of sight in the above equation. A closely related quantity is shear γ which, along with the convergence, makes up elements of a 2×2 matrix whose components define the distortion of an image at any point on the sky.

Transforming the convergence to harmonic space and assuming statistical isotropy, one obtains the convergence power spectrum $P^{\kappa\kappa}$, defined as (e.g., Huterer 2023)

$$\langle \kappa_{\ell m} \kappa_{\ell' m'} \rangle = \delta_{\ell\ell'}\, \delta_{mm'}\, P^{\kappa\kappa}(\ell), \tag{18}$$

where the multipole ℓ correspond to an angle $\theta \simeq 180^\circ/\ell$. The convergence power spectrum is identical to the shear power spectrum in the limit of weak distortions (i.e., in the weak-lensing limit); $P^{\gamma\gamma}(\ell) \simeq P^{\kappa\kappa}(\ell)$. For a Gaussian field, either $P^{\gamma\gamma}$ or $P^{\kappa\kappa}$ would contain all information. Because the weak-lensing field is nongaussian on small scales, higher-order correlations contain additional information and may be useful to exploit.

The convergence (or shear) power spectrum is related to theory in a straightforward way: it is a projection along the line of sight of the three-dimensional matter power spectrum $P(k)$. Here, we also assume weak-lensing *tomography* (Hu 2002)—slicing of the shear signal in redshift bins—which enables extraction of additional information from the weak-lensing shear, as it makes use of the radial information which is crucial for growth. Consider correlating shears in some redshift bin i to those in redshift bin j. Tomographic cross-power spectrum for these two redshift bins, at a given multipole ℓ, can be related to theory by starting with Eqs. (17) and (18); the result is

$$P_{ij}^{\kappa\kappa}(\ell) \simeq P_{ij}^{\gamma\gamma}(\ell) = \int_0^\infty dz\, \frac{W_i(z)\, W_j(z)}{r(z)^2\, H(z)}\, P\!\left(\frac{\ell}{r(z)}, z\right). \tag{19}$$

Here, the weights W_i are given by

$$W_i(\chi) \equiv \frac{3}{2}\, \Omega_{\rm M} H_0^2\, q_i(\chi)\, (1+z), \tag{20}$$

where

$$q_i(\chi) \equiv r(\chi) \int_\chi^\infty d\chi_{\rm S} n_i(\chi_{\rm S}) \frac{r(\chi_{\rm S} - \chi)}{r(\chi_{\rm S})}, \tag{21}$$

and n_i is the normalized ($\int n(z) dz = 1$) comoving density of galaxies if the coordinate distance $\chi_{\rm S}$ falls in the distance range bounded by the ith redshift bin, and zero otherwise. Further, $r(z)$ is the comoving distance and $H(z)$ is the Hubble parameter. Note that the weights W_i are purely geometrical, and do not contain any growth information. The key takeaway from Eq. (19) is that weak-lensing convergence power spectrum is proportional to the matter power spectrum $P(k)$, and hence (on linear scales) to the growth squared, $D(z)^2$, but without the complicating presence of galaxy bias.

Weak lensing, therefore, offers particularly good prospects for constraining the growth of structure. With N tomographic bins, one has a total of $N(N+1)/2$ tomographic bin pairs, each of which contains cosmological information. For typical surveys $N \simeq$ 5-10, enabling in principle the constraints on the growth of structure $D(z)$ with relatively fine temporal resolution.

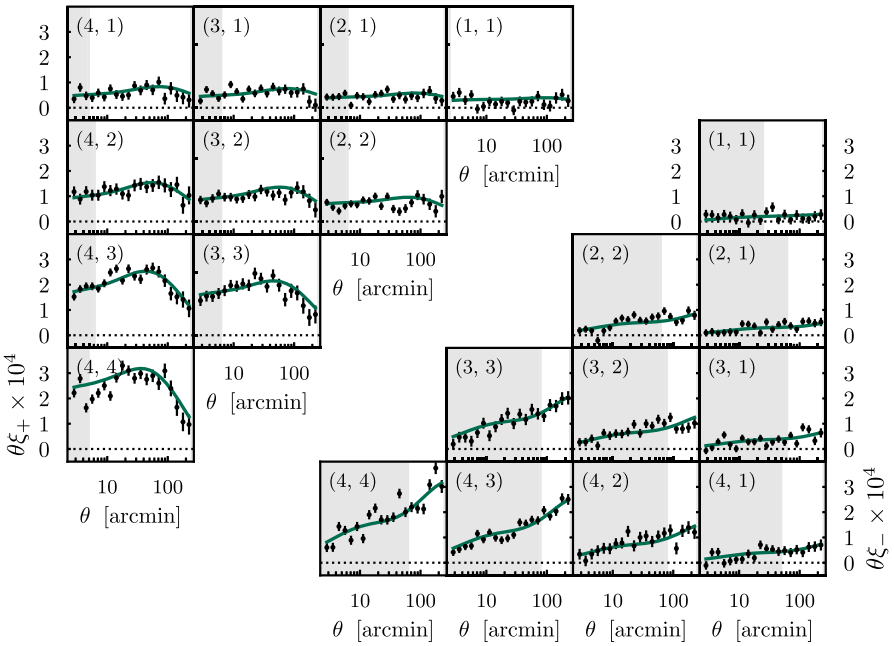

Fig. 2 Tomographic shear measurements of the 2-point correlation function of shear in real space, $\xi_{\pm}^{ij}(\theta)$ from the Year-3 data analysis of the Dark Energy Survey. The pair of numbers in ξ (written in the top left corner of each panel) refers to the pair of redshift bins from which the measurement is made (e.g., "2,4" means spatial correlation of galaxies in bin 2 to those in bin 4). The plots above the diagonal show $\theta\xi_+^{ij}(\theta)$ as a function of θ, while those below show $\theta\xi_-^{ij}(\theta)$. The curvy solid line shows the best-fit ΛCDM model. The gray regions show scales *not* used in the final parameter constraints due to concerns about modeling of the non-linear clustering at these smaller scales. Image adapted from DES Y3 shear analysis (Secco et al. 2022), copyright by APS

Modern measurements of the tomographic power spectrum of weak lensing shear, adopted from the Dark Energy Survey (DES; Secco et al. 2022), are shown in Fig. 2. Note that the figure shows the real-space shear correlation functions $\xi_{\pm}^{ij}(\theta)$ (multiplied by θ for readability) for any two tomographic bins i and j. These real-space correlation functions are just harmonic transforms of the convergence power spectrum $P_{ij}^{\kappa}(\ell)$, and are used because the weak-lensing measurements are often performed in real space (in θ), rather than in multipole space (in ℓ). The real-space correlation functions are obtained from the convergence power spectrum via

$$\xi_{\pm}^{ij}(\theta) = \frac{1}{2\pi}\int_0^{\infty} P_{ij}^{\kappa}(\ell) J_{0,4}(\ell\theta)\ell d\ell, \tag{22}$$

where $J_{0,4}(x)$ is the Bessel function of zeroth and fourth order, respectively. Note the impressive agreement between the shear measurements and the best-fit ΛCDM model in Fig. 2, extending even to the scales that were conservatively not used in the cosmological analysis (shaded in gray).

There are also important systematic errors that enter weak-lensing measurements. Notably, shear measurements are in general challenging, and are impacted by smearing of galaxy shapes by atmospheric distortions or other instrumental artifacts. Intrinsic alignments between source galaxies (Catelan et al. 2001; Hirata and Seljak 2004) complicate theoretical predictions and need to be explicitly modeled. Finally, photometric redshifts of source (and lens) galaxies have complex statistical properties that need to be corrected for where possible, then explicitly modeled in the analysis. For a review of these and other issues, see Mandelbaum (2018).

3.3 Galaxy-shear cross-correlations and 3×2 analysis

In addition to measuring shapes of distant galaxies across the sky and correlating them, there are other ways to leverage weak-lensing observations to learn about the growth of structure in the universe. One option is to measure the correlation of the *shears* of background galaxies with the *positions* of the foreground galaxies. This correlation is known under the name *galaxy–galaxy lensing*, and effectively measures the lensing efficiency of foreground galaxies. The method should perhaps be called galaxy–galax*ies* lensing, as it correlates the position of one foreground galaxy with the shapes of a number of background galaxies that are near it on the sky. Another better name is *galaxy–shear cross-correlation*, as galaxy positions are correlated with (other galaxies') shear.

Modern analyses combine the galaxy clustering (galaxy–galaxy correlations), cosmic shear (shear–shear correlations), and galaxy–galaxy lensing (galaxy–shear correlations) into one unified analysis. This combination goes under the informal name of "3 × 2" analysis, named for three two-point correlation functions.

If the actual observations were made in a single redshift bin and on a single spatial scale, then they would correspond to the data vector of three elements, $[gg, g\gamma, \gamma\gamma]$, where g stands for galaxy position, and γ for cosmic shear. Because the observations span a number of redshifts and scales, the resulting data vector can be much longer. For example, in the DES Y3 analysis (Abbott et al. 2022), the full data vector contains about 1000 elements, corresponding to measurements of gg, $g\gamma$, or $\gamma\gamma$, evaluated at a number of spatial scales k and in several redshift bins. About half of these measurements were made on linear or quasi-linear scales where theoretical modeling is accurate and were used to constrain cosmological parameters.

Because a 3 × 2 analysis efficiently combines observations of galaxy clustering and gravitational lensing, it also serves as a major probe of the growth of structure. The constraints on growth from a 3 × 2-type analysis are not trivial to isolate; we will discuss in Sect. 4.2 how this can be done. Instead, we typically quote constraints on the combination of the amplitude of mass fluctuations and matter density that is well constrained by galaxy clustering and weak lensing[4]

[4] Note that S_8 depends on redshift because $S_8(z) \propto \sigma_8(z) \propto D(z)$; recall Eq. (16). Conventionally, the redshift-dependent part is taken out to quote constraints on S_8 at $z = 0$.

$$S_8 \equiv \sigma_8 \sqrt{\frac{\Omega_{\rm M}}{0.3}}. \tag{23}$$

Constraints on S_8 are then roughly interpreted as those on the growth of cosmic structure. In Sect. 3.7 below, we show a compilation of current constraints on S_8 from current data.

3.4 Counts of galaxy clusters

The abundance of clusters of galaxies as a function of their mass and redshift is very sensitive to cosmic growth. Galaxy clusters are the observed baryonic components of dark-matter *halos*, so the abundance of clusters can often be quantified via our theoretical understanding of the abundance of halos. The halo abundance formalism can be studied from first principles using the excursion-set formalism pioneered by Bond et al. (1991) and reviewed by Zentner (2007). In this formalism, formation of a halo occurs when random walk of overdensity δ, as a function of radius of a sphere over which it is evaluated, crosses some critical threshold. This threshold is quoted in terms of the peak height $\nu(M) \equiv \delta_c/\sigma(M)$, where $\delta_c \simeq 1.686$ is the critical overdensity for collapse and σ is the amplitude of mass fluctuations defined in Eq. (16). Because halo formation is exponentially sensitive to the peak height (in the simple spherical-top-hat-overdensity model), and $\nu(z) \propto 1/\sigma(z) \propto 1/D(z)$, the sensitivity of the halo abundance to the growth of structure is very strong.

Because galaxy clusters are the most massive collapsed objects in the universe, they are described by the density field in the not-overly non-linear regime. As a consequence, their abundance can be modeled analytically, using arguments first laid out by Press and Schechter (1974) that preceded those of the more general (and aforementioned) excursion-set formalism, and with a rather transparent dependency on the cosmological parameters (Allen et al. 2011; Haiman et al. 2000). The quantity that describes the abundance of galaxy clusters is the mass function, which is the space density at arbitrary redshift and mass, $n(z, M)$, and is typically reported as the number per unit log interval in mass, $dn/d\ln M$. The number of clusters with mass above $M_{\rm min}$ and below redshift $z_{\rm max}$ in some volume of solid angle $\Omega_{\rm sky}$ is then

$$N(z<z_{\rm max}, M > M_{\rm min}) = \Omega_{\rm sky} \int_0^{zmax} dz \int_{M\,min}^{\infty} \frac{dn}{d\ln M} \frac{r^2(z)}{H(z)} d\ln M, \tag{24}$$

where $r^2(z)/H(z) = dV/(d\Omega dz)$ is the volume element, with r the comoving distance and H the Hubble parameter. In practice, the number of clusters is evaluated by connecting it explicitly to directly observable quantities (as discussed near the end of this subsection), but the mass function retains its central role in connecting observations with theory, and its strong dependence on the growth of structure remains useful.

While the cutting-edge approach for modeling the mass function is to calibrate it directly on simulations and interpolate in space of cosmological parameters using a so-called emulator (McClintock et al. 2019; Nishimichi et al. 2019; Bocquet et al. 2020), here we stick with the semi-analytical mass function for illustrative purposes.

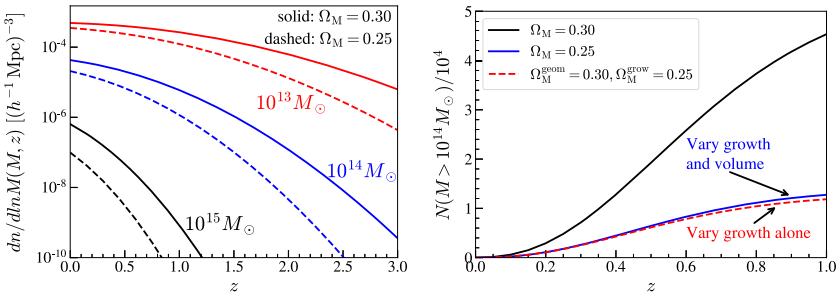

Fig. 3 Sensitivity of galaxy cluster counts on growth. The left panel shows the Tinker et al. (2008) mass function, as a function of redshift, for $M = 10^{13}, 10^{14}$, and $10^{15}\, M_\odot$. The right panel shows the number of clusters expected above $M = 10^{14}\, M_\odot$ out to redshift z, assuming a survey covering 5000 sq. deg (note that the y-scale shows counts in units of 10^4). The right panel shows that the sensitivity of number counts on cosmology comes largely through growth, since changing the growth alone (and keeping geometrical terms unchanged) accounts for most of the difference when moving to a new cosmological model—here, a different value of Ω_M

We adopt the Tinker et al. (2008) mass function, which has been shown to be accurate to $\sim 5\%$ over a respectably wide range of mass and redshift. The Tinker mass function is defined as dM and dz as

$$\frac{dn}{d\ln M} = f(\sigma)\frac{\rho_{M,0}}{M}\frac{d\ln\sigma^{-1}}{d\ln M}$$
$$f(\sigma) = A\left[\left(\frac{\sigma}{b}\right)^{-a} + 1\right]e^{-c/\sigma^2}, \tag{25}$$

where $\rho_{M,0}$ is the matter density today, σ is the amplitude of mass fluctuations, and a, b, and c are redshift-dependent coefficients calibrated from simulations and reported in Tinker et al. (2008). Moreover, M refers to halo mass specifically defined as the mass in a spherical region with 200 times the mean mass density in the universe. Here, the growth function dependence enters through the amplitude of mass fluctuations $\sigma(M,z) \propto D(z)$ which is found in the exponential, as predicted by the Press–Schechter (and, more generally, excursion-set) arguments.

In Fig. 3, we show the sensitivity of the cluster counts on the growth of structure. The left panel shows the Tinker mass function vs. redshift for three values of mass ($M = 10^{13}, 10^{14}$, and $10^{15}\, M_\odot$), and for two values of matter density Ω_M. It shows strong dependence of the expected number density of clusters on the matter density, which in turn determines the growth of structure. The right panel shows the number of clusters expected above $M = 10^{14}\, M_\odot$ out to redshift z, assuming a survey covering 5000 sq. deg (note that the y-scale shows counts in units of 10^4). We observe that the sensitivity of number counts on cosmology comes largely through growth, rather than the geometrical volume factor. This explicitly illustrates the fact that cluster counts are very sensitive probes of growth (Bahcall and Fan 1998; Haiman et al. 2000; Mullis et al. 2005; Brodwin et al. 2010; Holz and Perlmutter 2012; Kravtsov and Borgani 2012; Mortonson et al. 2011; Jee et al. 2014)

Because cluster masses are not directly measured, modern measurements of the abundance of clusters are typically compared to theory not in terms of their masses, but rather other intermediate, more readily observable quantities called mass "proxies". One such mass proxy is "richness", defined as the number of galaxies that reside in a cluster. Other mass proxies include X-ray flux or weak-lensing signal measured toward clusters; all of these proxies correlate with cluster mass. Conversion from noisy measurements of mass proxies to actual cluster masses introduces both statistical and systematic errors, and controlling and quantifying these errors—especially the systematics— is the principal challenge for cluster cosmology. If the systematics can be controlled and understood, then the prospects for constraining the growth of structure via cluster abundance with ongoing or upcoming wide-field cosmological surveys such as eROSITA, LSST, and Euclid and Nancy Roman Space Telescopes are very good.

3.5 Cosmic velocities

Cosmic velocities are also sensitive to the growth of structure. In linear theory, the velocity $\mathbf{v}$ is directly related to overdensity δ via the continuity equation which reads

$$\mathbf{v} = \frac{i\mathbf{k}}{k^2}\frac{D'}{D}\delta = \frac{i\mathbf{k}}{k^2}afH\delta, \tag{26}$$

where the prime denotes a derivative with respect to conformal time η, and the second equality follows because $' = d/d\eta = a(d/dt) = aH(d/d\ln a)$. Here, we have defined the growth rate f as

$$f \equiv \frac{d\ln D}{d\ln a}. \tag{27}$$

Then, the velocity power spectrum can be related to the matter power spectrum in linear theory via

$$P_{vv}(k,a) = \left[\frac{af(a)H(a)}{k}\right]^2 P(k,a). \tag{28}$$

Note a key feature: the velocity power spectrum not only scales as the matter power spectrum (and hence the usual growth term $D(a)$ squared), but also is further proportional to the square of the growth rate $f(a)$. Because the growth rate is sensitive to both the standard cosmological parameters (Ω_M and w, for example) and modified gravity, this latter dependence makes the cosmic velocities particularly well suited to cosmological tests that rely on the growth of structure (Song and Percival 2009).

Probably the most prominent method for utilizing the velocities are the redshift-space distortions (RSD). The RSD take place because redshift of galaxies is affected by their gravitational infall into nearby large-scale structures, as well as by the galaxies' own peculiar velocities. Because we typically measure the galaxies' redshifts in order to get their radial location, clustering measurements in redshift space are subject to RSD. There are two RSD effects—the so-called Kaiser effect, and fingers of god; see Fig. 4. To lowest order, the redshift-space matter power

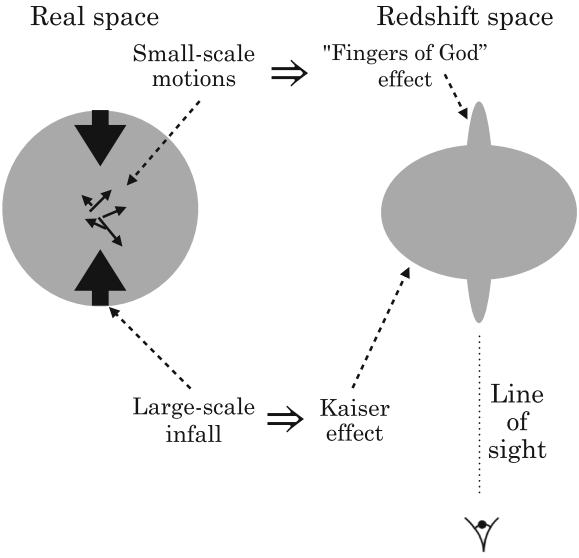

Fig. 4 Illustration of the redshift-space distortions. There are two principal effects: (1) On large scales, velocity flows into large overdensities, "squishing" the appearance of the object along the line of sight; this is the Kaiser effect; (2) On smaller scales, random motions introduce apparent elongation along the line of sight; this is the somewhat hyperbolically called "fingers of god" effect. Image adapted from Huterer (2023)

spectrum $P(\mathbf{k})^{(s)}$ is related to the isotropic matter power spectrum $P(k)$ via (e.g., Song and Percival 2009)[5]

$$P(\mathbf{k},z)^{(s)} = \left[b + f\mu^2\right]^2 F(k^2\sigma_v^2\mu^2)P(k,z), \tag{29}$$

where the superscript $^{(s)}$ indicates that we are referring to clustering in redshift space. Here, μ is the cosine of the angle between the line-of-sight direction and wavenumber $\mathbf{k}$, $b = b(k,z)$ is the galaxy bias, $f = f(z)$ is the growth rate, and $P(k, z)$ is the isotropic part of the matter power spectrum. Finally, the function $F(k^2\sigma_v^2\mu^2) \simeq 1/(1 + k^2\sigma_v^2\mu^2)$ models the suppression of the redshift-space power spectrum at high k in terms of the velocity dispersion σ_v, which is a free parameter that generally depends on halo mass and redshift.

The RSD effects can be readily measured in spectroscopic surveys where accurate galaxy redshifts are available. Because $P(\mathbf{k})^{(s)}$ has terms that go as μ^0, μ^2, and μ^4 (in linear theory), we can respectively measure the monopole, quadrupole, and hexadecapole of redshift-space galaxy clustering.

An alternative to utilizing the RSD to probe growth is to measure the velocities directly. Redshift to a galaxy is affected by its velocity, so accurate measurements of the former can constrain the latter, and hence cosmic growth. Velocity of a galaxy at a physical distance $\mathbf{x}$ is

[5] A slightly more accurate formulation replaces the density power spectrum $P(k,z) \equiv P_{\delta\delta}$ on the right-hand side of Eq. (29) with a combination of $P_{\delta\delta}$, the velocity power spectrum P_{vv}, and the cross-power $P_{\delta v}$, as (de la Torre and Guzzo 2012)

$$P(\mathbf{k},z)^{(s)} = \left[b^2P_{\delta\delta} + 2bf\mu^2P_{\delta v} + f^2\mu^4P_{vv}\right]F(k^2\sigma_v^2\mu^2).$$

$$\dot{\mathbf{x}} = \frac{d}{dt}(a\mathbf{r}) = \dot{a}\mathbf{r} + a\dot{\mathbf{r}} = H\mathbf{x} + \mathbf{v}_{\rm pec}, \tag{30}$$

where $\mathbf{r}$ is the comoving distance, H is the Hubble parameter, and $\mathbf{v}_{\rm pec}$ is the component of the peculiar velocity of the galaxy parallel to the line of sight. Specializing in $z \ll 1$ (and ignoring 2nd-order terms in redshift), we get the relation between the observed redshift $z_{\rm obs}$ and true redshift z as

$$cz_{\rm obs} \simeq cz + v_{\rm pec}. \tag{31}$$

The effect of peculiar velocities is non-negligible only for very nearby galaxies; consider that for a galaxy at $z \simeq 0.03$, $cz \simeq 10,000\ {\rm km}\,s^{-1}$, while the typical peculiar velocity is $v_{\rm pec} \simeq 200\ {\rm km}\,s^{-1}$.

To determine the peculiar velocity, we need the observed redshift and distance. Galaxy redshift can be determined by taking a sufficiently high-resolution spectrum of the galaxy, and is in principle straightforward. Measuring the distance to a galaxy is far more challenging. To get the distance, one may use an empirical fundamental-plane relation that relates an object's distance to its surface brightness. Alternatively, one can use type Ia supernovae, standard candles whose distances can be determined by measuring their fluxes and adopting the fact that these objects have nearly equal luminosities. In surveys thus far, the fundamental-plane measurements are available for $\sim$10,000 galaxies and give distances accurate to $20-30\%$ per object. Type Ia supernovae are more accurate ($\sim 10\%$ per object), but available for fewer galaxies (typically $\lesssim$500) in extant peculiar-velocity surveys. Either method allows a noisy measurement of individual galaxies' peculiar velocities; their correlations are sensitive to growth as indicated in Eq. (28). Recent observational efforts, combined with modern distance calibrations, have been greatly increasing the number of galaxies and supernovae available for peculiar-velocity tests of cosmology (Howlett et al. 2022; Tully et al. 2023).

For practical reasons having to do with patchy sky coverage and sparsity of source galaxies, one often measures the (configuration-space) *correlation function* of galaxy velocities. The correlation function C_{vv} is proportional to the velocity power spectrum. Since the velocity power spectrum is proportional to the quantity $f\sigma_8 \equiv f(z)\sigma_8(z)$

$$P_{vv}(k,z) \propto f^2(z)P(k,z) = f^2(z)\sigma_8^2(z)P(k,z=0), \tag{32}$$

so is the velocity correlation function

$$C_{vv} \propto P_{vv} \propto (f\sigma_8)^2. \tag{33}$$

This relation explains why the results from the analyses of cosmic velocities are often framed as constraints on the quantity $f\sigma_8$, evaluated in redshift bins. Note, however, that, while the strongest dependence of velocity correlations is on the quantity $f\sigma_8$, most of the standard cosmological parameters also enter, mainly via their impact on $P(k)$ that is not captured by σ_8. This complicates attempts to isolate the measurements on $f\sigma_8$, as these other parameters (e.g., the physical baryon density $\Omega_b h^2$ or the

spectral index n_s) need to be given priors from other data, or else be simultaneously constrained by the velocities.

Observing the peculiar velocities of nearby galaxies or type Ia supernovae that they host is not the only way to probe the galaxy velocity field. One useful probe in this regard is the *kinetic SZ effect* (kSZ). The kSZ is caused by galaxy clusters' peculiar velocities in the CMB rest frame. A cluster with peculiar velocity $v_{\rm pec,\parallel}$ along the line of sight will incur a density shift of the CMB temperature in the direction of the cluster of

$$\left(\frac{\delta T}{T}\right)_{\rm kSZ} \simeq -\tau_e \frac{v_{\rm pec,\parallel}}{c}, \tag{34}$$

where τ_e is the optical depth for electron scattering in the cluster. The kSZ modifies the blackbody spectrum of an object by the temperature shift given in Eq. (34). For typical values $\tau_e \simeq 0.01$ and $v_{\rm pec} \simeq 500\,{\rm km}\,s^{-1}$, the kSZ fractional temperature shift is on the order of the primordial temperature anisotropy ($\sim 10^{-5}$) and thus quite small. The kSZ effect was first detected about a decade ago (Hand et al. 2012), and its better mapping will allow us to probe the velocity field of galaxy clusters, and hence the growth of cosmic structure.

3.6 Role of the CMB

Being a snapshot of the universe at $z \simeq 1000$, the cosmic microwave background (CMB) naively does not have much information about the growth of structure. Specifically, we are most interested in the growth at relatively low redshift, $z \lesssim 2$, where growth slowly transitions from being robust in the dark-matter dominated regime, to being strongly suppressed as dark energy starts to dominate,[6] and we certainly do not expect that the CMB be informative at such a low redshift. While technically correct, these expectations need to be modulated with the fact that the CMB is nevertheless extremely important in pinning down the initial amplitude of the power spectrum (that is, the parameter A_s in Eq. (14)). This constraint, along with the *present*-day clustering amplitude (measured as σ_8 or S_8), allows a significant improvement in the precision of constraints on the growth of structure.

CMB contributes in other ways. Notably, CMB *lensing*—measured as subtle displacements in the distribution of hot and cold spots on arcminute scales—is sensitive to the growth of structure. CMB lensing is described by the power spectrum of the deflection signal of photons as they cross large-scale structure traveling toward our detectors. Mathematically, the CMB lensing power spectrum looks similar to the weak-lensing shear power spectrum in Eq. (19); the main difference is that kernel of the shear power spectrum peaks at $z \sim 0.5$, while that of CMB lensing peaks at $z \sim 3$. Hence, CMB lensing in principle helps probe the growth of structure at a redshift higher than galaxy or weak-lensing surveys. The signal-to-noise of CMB lensing is currently limited, but future measurements from surveys like Simons Observatory and CMB-S4 may provide interesting constraints on the growth of structure in their

[6] In the concordance ΛCDM model with 30% matter and 70% dark energy, the energy densities in these two components are equal at $z \simeq 0.33$.

own right. Another promising direction is to cross-correlate the CMB map with a galaxy map; the contribution of CMB lensing should lead to a sufficiently high signal-to-noise to probe the growth of structure (Hu 2002; Peacock and Bilicki 2018; Wilson and White 2019; Krolewski et al. 2020; García-García et al. 2021).

3.7 Cosmological constraints on $f\sigma_8$ and S_8

Having reviewed the principal cosmological probes of growth, we now summarize current constraints. While the temporal evolution growth enters many of the observable quantities in cosmology, isolating it is in general not straightforward; we discuss such strategies in Sect. 4 below. Instead, the majority of the cosmological analyses assume that growth is modeled according to the assumed cosmological model (e.g., ΛCDM and its variants, or else modified gravity), and report the constraints on the parameters of that model, say $\Omega_{\rm M}$ and σ_8. To present results in a more "model-independent" way, these surveys report constraints on derived cosmological parameters that are fairly directly related to what is being measured, yet contain information that in large part comes from growth. We now discuss these constraints.

Perhaps the most direct constraint comes from peculiar-velocity and redshift-space-distortion measurements, both of which are sensitive to the quantity $f\sigma_8$ at some effective redshift that depends on the distribution of source galaxies (see Eqs. (28) and (33)). The quantity $f\sigma_8$ depends on both growth and other cosmological parameters, principally via how they enter the matter power spectrum. Despite some degeneracy with these other parameters, the dependence on growth is very strong because both $f(z)$ and $\sigma_8(z)$ are directly related to the linear growth $D(z)$; $f\sigma_8 \propto (d\ln D/d\ln a)D$.

Constraints on $f\sigma_8$ from current measurements are shown in Fig. 5. The black error bars denote constraints from peculiar velocities (or their combination with clustering) at $z \simeq 0$; the points are mutually offset horizontally for clarity. From left to right, these peculiar-velocity constraints come from: type Ia supernovae from the 2 M++ compilation (Boruah et al. 2020), supernova distances from Supercal compilation and Tully–Fisher distances from 6dFGRS (Huterer et al. 2017), combination of galaxy velocities and galaxy clustering applied to 6dFGRS (Turner et al. 2023), and combination of galaxy velocities from 6dFGRS and SDSS with velocity and density predictions from 2 M++ galaxy survey (Said et al. 2020). The other constraints, at higher redshift, are mainly from redshift-space distortion modeling of galaxy samples. These RSD constraints come from: 6dFGRS (Beutler et al. 2012), GAMA (Blake et al. 2013), WiggleZ (Blake et al. 2012), VIPERS (Pezzotta et al. 2017), SDSS main galaxy sample (MGS) (Howlett et al. 2015), FastSound on Subaru (Okumura et al. 2016), and BOSS+eBOSS (Alam et al. 2021). We see that the $f\sigma_8$ constraints are in a good agreement with the predictions of the currently favored ΛCDM model. Particularly notable is the complementarity between the different probes, as peculiar velocity surveys measure motions of galaxies at distances $r \lesssim 100\,h^{-1}$Mpc, and thus very low redshift ($z \simeq 0.02$), while the RSD

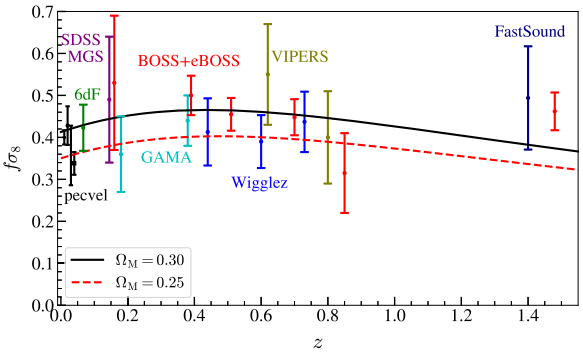

Fig. 5 Constraints on $f\sigma_8 \equiv f(z)\sigma_8(z)$. The curves show predictions from ΛCDM with two alternate values of the matter density—the fiducial $\Omega_M = 0.3$, and also $\Omega_M = 0.25$. The errors show the various extant measurements, as follows. The black error bars denote constraints from peculiar velocities (or their combination with clustering) at $z \simeq 0$; these black points are mutually offset horizontally for clarity. From left to right, these peculiar-velocity constraints come from: type Ia supernovae from the 2 M++ compilation (Boruah et al. 2020), supernova distances from Supercal compilation and Tully–Fisher distances from 6dFGRS (Huterer et al. 2017), combination of galaxy velocities and galaxy clustering applied to 6dFGRS (Turner et al. 2023), and combination of galaxy velocities from 6dFGRS and SDSS with velocity and density predictions from 2 M++ galaxy survey (Said et al. 2020). The other constraints, at higher redshift, come from redshift-space distortion modeling of galaxy samples; see text for details

measurements probe growth to galaxies and quasars at a much higher redshift, all the way up to $z \simeq 1.5$ for current surveys.

In contrast to peculiar-velocity and RSD measurements, constraints from weak-lensing surveys and measurements of the broadband galaxy-clustering power spectrum are not very sensitive to the growth rate f or the combination $f\sigma_8$, but rather on the overall amplitude of matter fluctuations. This amplitude is larger if either matter density Ω_M or the amplitude of mass fluctuations σ_8 increases. Therefore, the constraints typically look like a banana-shaped region in the $\Omega_M - \sigma_8$ plane, indicating their mutual anti-correlation. To decouple these two parameters, the constraints are often reported on their combination $S_8 \equiv \sigma_8(\Omega_M/0.3)^{0.5}$ that is very well constrained. Note that σ_8 and S_8 explicitly refer to the value of these quantities at redshift zero, to which the weak-lensing and galaxy-clustering are extrapolated by convention, in contrast to peculiar-velocity and RSD constraints which are traditionally quoted as $f\sigma_8 \equiv f(z)\sigma_8(z)$.

Figure 6 shows the constraints on S_8. Going top to bottom, the first three measurements come from CMB analyses: temperature-only analysis from Planck (Aghanim et al. 2020; also shown as a vertical shaded region), temperature+polarization+lensing analysis from Planck (Aghanim et al. 2020), and temperature+polarization information from ACT combined with large-scale temperature from WMAP (Aiola et al. 2020). Going further down, we show the constraints of select large-scale structure combinations as follows. The black error bars show constraints from the fiducial 3×2 analysis from DES Y3 (Abbott et al. 2023a), DES Y3 with cosmic shear alone (Amon et al. 2022; Secco et al. 2022), and DES 3×2 with the

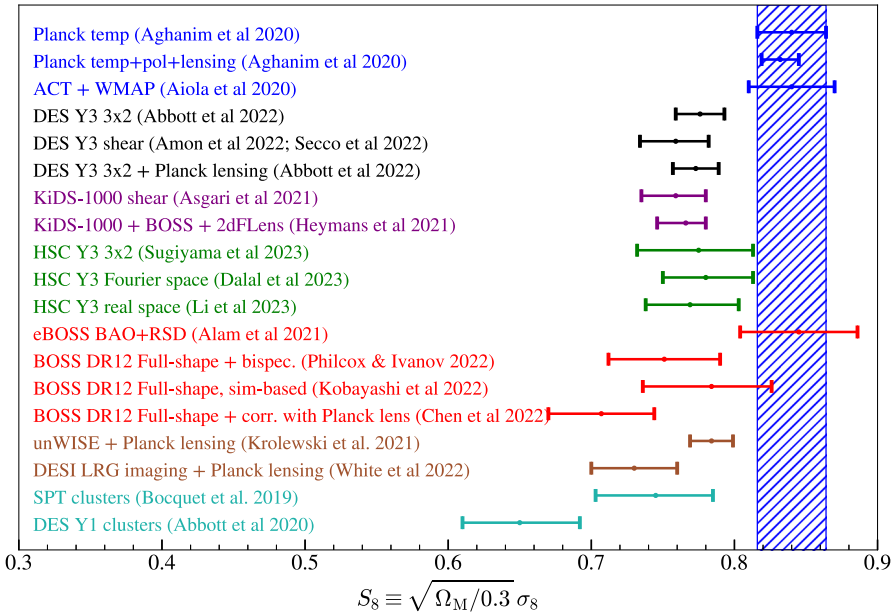

Fig. 6 Constraints on $S_8 \equiv \sigma_8\sqrt{\Omega_M/0.3}$ from various analyses. Going top to bottom, the first three measurements come from the CMB analysis: temperature-only analysis from Planck (Aghanim et al. 2020, also shown as a vertical shaded region), temperature + polarization + lensing analyses from Planck (Aghanim et al. 2020), and temperature + polarization information from ACT combined with large-scale temperature from WMAP (Aiola et al. 2020). All of the other constraints involve some combination of large-scale structure probes, see text for a detailed description. All constraints assume the fiducial ΛCDM model. The error bars show 68% credible intervals, which are asymmetric around the mean in some cases

addition of Planck lensing information (Abbott et al. 2023b). The purple error bars show constraints from KiDS-1000 (Asgari 2021) and KiDS-1000 combined with clustering from BOSS and galaxy-galaxy lensing in the overlap region of KiDS, BOSS and 2dFLens (Heymans 2021). The green error bars show the constraints from the Hyper Suprime-Cam (HSC) year-3 data analysis: their 3×2 analysis result (Sugiyama et al. 2023), and their Fourier-space (Li et al. 2023) and real-space (Dalal et al. 2023) shear-only constraints. The red error bars show constraints from the combined BAO and RSD information from BOSS+eBOSS (Alam et al. 2021), from the emulator-based full-shape analysis from BOSS DR 12 (Kobayashi et al. 2022), full-shape BOSS DR12 analysis combined with the BOSS DR12 bispectrum monopole (Philcox and Ivanov 2022), and full-shape BOSS DR12 along with its cross-correlations with Planck lensing (Chen et al. 2022). The brown error bars show combination of unWISE galaxy clustering and Planck lensing (Krolewski et al. 2021), and clustering of luminous red galaxies from DESI imaging survey combined with Planck lensing (White et al. 2022). The turquoise error bars show constraints from the abundance of galaxy clusters as measured by South Pole Telescope (Bocquet et al. 2019) and DES Year-1 data (Abbott et al. 2020). All constraints assume the fiducial ΛCDM model.

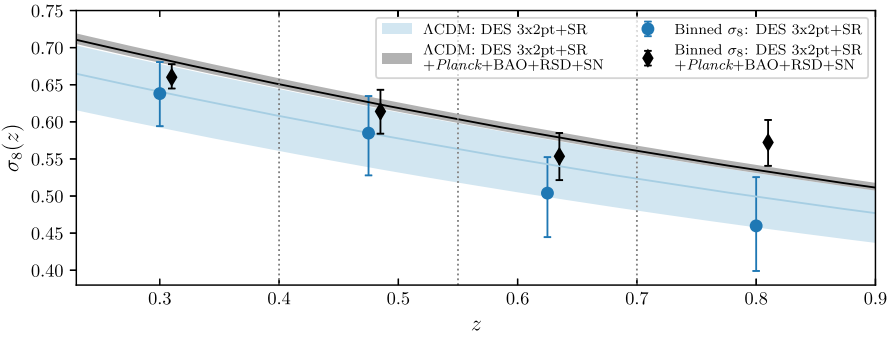

Fig. 7 Constraints on the time-dependent amplitude of mass fluctuation $\sigma_8(z)$ and comparison with theory. The blue points show the constraints from DES 3 × 3 analysis alone in each of the four lens redshift bins. The black points show constraints from the combination of DES 3 × 3 and external data (Planck, BAO, RSD, SN), along with the shear ratio statistic from DES (labeled SR). Lines and shaded bands show the means and 68% credible intervals inferred from ΛCDM posteriors corresponding, respectively, to DES alone (blue), and DES plus external data (black). Image reproduced with permission from Abbott et al. (2023a), copyright by APS

The most apparent trend in Fig. 6 is the so-called[7] "S8 tension", which reflects the fact that CMB measurements show a higher amplitude of mass fluctuations than lensing surveys. Planck's temperature, polarization, and lensing information combined indicate $S_8 = 0.832 \pm 0.013$, and the combination of ACT and WMAP give a consistent result ($S_8 = 0.840 \pm 0.040$). Lensing surveys, on the other hand, typically show a lower value of this parameter, exemplified by DES Y3 constraint $S_8 = 0.775 \pm 0.017$ and a very similar constraint from KiDS ($S_8 = 0.759^{+0.024}_{-0.021}$). Similar trends are seen with cluster abundance constraints. Future data will sharply improve the constraints on growth.

Constraints on σ_8 or S_8 are typically projected to, and reported at, redshift zero. One can do better, however, and constrain the temporal evolution of the (linear) amplitude of mass fluctuations, with the understanding that these amplitude parameters are directly proportional to the linear growth function $D(z)$. Such constraints are shown in Fig. 7, adopted from DES Y3 extended-model paper (Abbott et al. 2023a). The blue points show the constraints from DES 3 × 3 analysis alone in each of the four lens redshift bins. The black points show constraints from the combination of DES and external data: CMB, baryon acoustic oscillations (BAO), redshift-space distortions (RSD), and type Ia supernovae (SN). Lines and shaded bands show the mean and 68% credible interval inferred from ΛCDM posteriors corresponding respectively to DES alone, and DES plus external data. Clearly, $\sigma_8(z)$ measurements are already accurate, especially when various datasets are combined, and sharply test (and, thus far, are in agreement with) the standard ΛCDM cosmological model.

[7] Also referred to as the "σ_8 tension", as a similar trend is seen in constraints on σ_8.

4 Consistency tests with growth

As mentioned in the Introduction, growth of structure owes its outsize importance chiefly to the fact that it is a powerful discriminator between models of dark energy, and that it is sensitive to the presence of modified gravity (e.g., Lue et al. 2004; Amendola et al. 2008). In Sect. 3 we discussed how individual probes are sensitive to growth, and in particular (in Sect. 3.7) how the contraints derived from growth are reported in the measurements of $f\sigma_8(z)$ and S_8. We now discuss more ambitious and direct uses of the information stored in the growth of structure, specifically how to utilize it to test classes of cosmological models.

4.1 Constraints on parameterized growth

While it is possible to isolate the constraints coming specifically from the growth of cosmic structure (as we discuss below in Sect. 4.2), this is typically not straightforward to implement. Moreover, such relatively general extractions of the growth information necessarily impose additional parameters that weaken the cosmological constraints. This is where a *simple* parameterization of growth becomes extremely useful. A successful such parameterization would have the ability to describe growth in ΛCDM and wCDM (where the equation of state of dark energy w is a free but constant parameter), as well as model departures expected in modified-gravity scenarios.

By far the most impactful parameterization of this kind is provided by "growth index" parameter[8] γ. This description of growth introduces a single, constant parameter defined in a phenomenological fit to the growth rate (Linder 2005)

$$f(a) \equiv \Omega_{\rm M}(a)^{\gamma}. \tag{35}$$

In other words, the linear growth factor is approximated by $D(a) = e^{\int_0^a d\ln a' \,[\Omega_{\rm M}(a')^{\gamma}]}$.

It has been known for a long time that the formula in Eq. (35) fits the linear growth very well for $\gamma \simeq 0.55$ (e.g., Peebles 1994; Wang and Steinhardt 1998). What is new here is that promoting γ to a free parameter enables describing growth in models far beyond the standard ΛCDM. Specifically, it has been shown that dynamical dark energy models where the equation of state ratio is parametrized as $w(a) = w_0 + w_a(1-a)$ are well fit by the growth index as long as it takes the value (Linder 2005)

$$\gamma = 0.55 + 0.02[1 + w(z=1)], \tag{36}$$

where $w(z=1)$ is the dark-energy equation of state evaluated at redshift one in this class of models. The form in Eq. (36) fits the exact linear rate to better than 0.3% when $w_0 + w_a < -0.1$ (Huterer and Linder 2007). A broad range of modified-gravity models, including time-varying gravity, DGP braneworld gravity (Dvali et al. 2000), and some scalar-tensor gravity, are fit accurately with the growth index (Linder and Cahn 2007).

[8] Not to be confused with shear which we discussed in Sect. 3.2.

There are other variants of parametrized growth. A more direct, and even less model-dependent, approach is to model $D(z)$ as a free function in redshift and interpolate it with principal components (Hu 2002), splines (García-García et al. 2021), or else with piecewise-constant values as done for $\sigma_8(z)$ in the DES Y3 extensions paper (Abbott et al. 2023a; see our Fig. 7). As the measurements of the growth of structure become more precise with upcoming surveys, such ambitious approaches will begin to return very interesting constraints and consistency-test results.

4.2 Comparing growth with geometry

Comparing measurements of geometric quantities to those describing the growth of structure is a particularly promising stress-test of the cosmological model (Zhang et al. 2005; Bernstein and Jain 2004; Ishak et al. 2006; Knox et al. 2006; Bertschinger 2006; Huterer and Linder 2007). For example, given constraints on the initial conditions (power spectrum shape and amplitude), very precise distance measurements from, e.g., type Ia supernovae (SNe Ia) and baryon acoustic oscillations (BAO) predict the convergence power spectrum measured by weak-lensing probes. Here, the weak-lensing signal depends on the late-time growth of structure, which in turn is precisely determined by distance measurements.

A straightforward way to compare geometry and growth, first proposed in the modern form and applied to early data by Wang et al. (2007), and then further developed by Ruiz and Huterer (2015), Bernal et al. (2016), Muir et al. (2021), Ruiz-Zapatero et al. (2021), Andrade et al. (2021), is to add additional cosmological parameters. Specifically, in the flat ΛCDM cosmological model one can take the matter density relative to the critical—which is normally encoded in one parameter, $\Omega_{\rm M}$—and duplicate it into two parameters: $\Omega_{\rm M}^{\rm geom}$ and $\Omega_{\rm M}^{\rm grow}$. One then modifies the theory code as follows: every geometrical term (for example, a distance formula) will depend on $\Omega_{\rm M}^{\rm geom}$, and every growth term (for example, in the growth-of-structure differential equation) will be fed $\Omega_{\rm M}^{\rm grow}$. With such an implementation, the tight relations linking geometry to growth in the standard cosmological model will be explicitly decoupled. In a flat cosmological model, the energy density of dark energy is given by $\Omega_\Lambda = 1 - \Omega_{\rm M}$, so such a split of $\Omega_{\rm M}$ is also automatically a split of Ω_Λ. One can extend such a geometry-growth split to models with more complicated dark-energy sectors. For example, in the analogous scenario of the flat wCDM model, the equation of state of dark energy, w, is also described by two parameters, $w^{\rm geom}$ and $w^{\rm grow}$. Therefore, a cosmological analysis with geometry-growth split is specified by

$$\bullet \ \text{split} \ \ \Lambda\text{CDM}: \quad \{\Omega_{\rm M}^{\rm geom}, \Omega_{\rm M}^{\rm grow}, \{p_i\}\}, \tag{37}$$

$$\bullet \ \text{split} \ \ w\text{CDM}: \quad \{\Omega_{\rm M}^{\rm geom}, \Omega_{\rm M}^{\rm grow}, w^{\rm geom}, w^{\rm grow}, \{p_i\}\}, \tag{38}$$

where $\{p_i\}$ are other, standard (and unsplit) cosmological parameters. Note that, while the implementation of the geometry-growth split may be ambiguous (i.e., it might be unclear whether a given term in a theory equation is "geometry" or "growth"), the geometry-growth test is always valid. This is because *any* mismatch

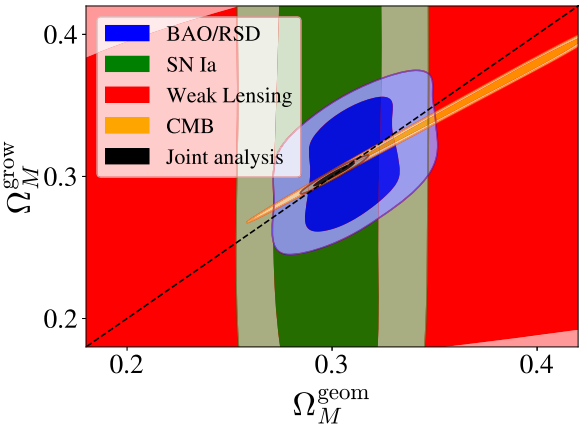

Fig. 8 Geometry-growth constraints from individual probes as well as the joint analysis. Here, we extend the wCDM model by assuming two parameters for the matter density relative to critical, $\Omega_{\rm M}^{\rm geom}$, which governs the geometrical quantities, and $\Omega_{\rm M}^{\rm grow}$, which controls the growth of structure; we also split the equation of state into $w^{\rm geom}$ and $w^{\rm grow}$, and marginalize over both of these parameters (and all others, unsplit parameters) in this figure. The dashed black line shows the consistency relation that is satisfied in the standard cosmological model, $\Omega_{\rm M}^{\rm geom} = \Omega_{\rm M}^{\rm grow}$. Note the impressive degeneracy breaking when the cosmological probes are combined. Image reproduced with permission from Andrade et al. (2021), copyright by IOP/Sissa

between geometry and growth terms—however, they are implemented—is disallowed in the standard (unsplit) cosmological model.[9]

Constraints on the geometry and growth parameters in the split wCDM model are shown in Fig. 8, adopted from Andrade et al. (2021). Here, we show the constraints on $\Omega_{\rm M}^{\rm geom}$ and $\Omega_{\rm M}^{\rm grow}$, marginalized over all other parameters, including $w^{\rm geom}$ and $w^{\rm grow}$. Note that SN Ia are manifestly sensitive to geometry only, and not to growth. The constraints from individual probes are necessarily weak, as the split parameter space contains severe parameter degeneracies. When the probes are combined, however, parameter degeneracies are broken and the constraints are strong.

Current constraints on geometry and growth indicate intriguing departures from the standard cosmological model (which predicts $\Omega_{\rm M}^{\rm geom} = \Omega_{\rm M}^{\rm grow}$ and $w^{\rm geom} = w^{\rm grow}$) with some combinations of datasets (Ruiz and Huterer 2015; Bernal et al. 2016; Andrade et al. 2021). These results will be well worth following up with forthcoming data.

4.3 Falsifying classes of models

Another very effective way to test the consistency of any given cosmological model is to:

- Start with constraints on the model that are provided by certain datasets or probes;

[9] Of course, it is a good idea to implement the separation between geometry and growth terms that is physically sensible.

- Compute what those parameter constraints imply for the larger space of observable quantities, for example cosmological functions $D(z)$, or $f\sigma_8(z)$ at an arbitrary redshift, or else derived parameters such as S_8; and then
- Test *those* predictions using new data or probes.

Such an approach has implicitly been discussed for a long time (e.g., Huterer and Linder 2007), but was first clearly spelled out by Mortonson et al. (2009) and applied to current data by Mortonson et al. (2010), Vanderveld et al. (2012), Miranda and Dvorkin (2018), Raveri (2020).

Falsification procedure as described above has a few clear advantages. First, the simple structure of smooth dark-energy models implies that, given current constraints, these models lead to very precise predictions for the temporal evolution of distance and growth at *all* redshifts, even well beyond the range probed by data used to impose the predictions. Second, those predictions are quite accurate not only for ΛCDM and wCDM, but also for models with a much richer dark-energy sector (Mortonson et al. 2009). This makes the predictions good targets for falsifying whole classes of models, particularly with data that probe new ranges of redshift (or new spatial scales) than those used to impose the predictions. Third, the ability to separately test growth and geometry comes about naturally in these tests, as predictions for both quantities as a function of redshift can be made straightforwardly, essentially by running the standard theoretical calculation constrained to the range of cosmological parameters allowed by current data.

We have already shown one example of predictions in this review; this is the Planck measurement of S_8, shown as the vertical band in Fig. 6. Note that the spirit of model predictions is at work here: even though S_8 is not a core parameter that CMB constrains, its value can be easily predicted by the CMB anisotropy measurements in a given cosmological model (here, ΛCDM). This prediction serves as a check against more direct S_8 measurements from galaxy clustering and weak lensing.

There are other ways to falsify models that are not quite as direct as the procedure described above. One such test is to compare the two gravitational potentials Ψ and Φ. Starting from the scalar-perturbed Friedmann–Robertson–Walker line element in the conformal Newtonian gauge

$$ds^2 = a^2(\eta)\left[(1+2\Psi)d\eta^2 - (1-2\Phi)\delta_{ij}dx_i dx_j\right], \tag{39}$$

the behavior of many cosmologically interesting modified-gravity theories can be fit with a free function of time and scale multiplying the Poisson equation, and another given by the ratio of Φ and Ψ. Specifically, one introduces two new functions of time[10] $\mu(a)$ and $\Sigma(a)$, defined as

$$\begin{aligned} k^2\Psi &= -4\pi G a^2(1+\mu(a))\rho\delta, \\ k^2(\Psi+\Phi) &= -8\pi G a^2(1+\Sigma(a))\rho\delta, \end{aligned} \tag{40}$$

where δ is the comoving-gauge density perturbation. Here, Σ parametrizes the

[10] We do not allow scale dependence of μ and Σ in the following discussion, although such scale dependence may be observable with future data; see, e.g., Hojjati et al. (2014).

change in the lensing effect on massless particles for a given matter field, while μ describes the change in the matter overdensity itself. Such a parameterization approximately describes a more complicated set of equations (Baker et al. 2013; Creminelli et al. 2009; Baker et al. 2011; Battye and Pearson 2012; Gleyzes et al. 2013, 2015; Bloomfield et al. 2013; Amendola et al. 2014; Hojjati et al. 2014), but has been numerically verified on scales of cosmological interest (Noller et al. 2014; Schmidt 2009; Zhao et al. 2011; Barreira et al. 2014; Li et al. 2013). Typically, one either assumes that μ and Σ are constant, or else that they scale with cosmic time under some parameterization (Caldwell et al. 2007; Abbott et al. 2019). Finally, there exist other, closely related, parameterizations of the gravitational potentials, including the E_G parameterization (Zhang et al. 2007) and parameterized post-Friedmannian framework (Hu and Sawicki 2007).

Because Σ determines the predictions for lensing, weak lensing measurements are primarily sensitive to this parameter but also have some smaller degree of sensitivity to μ via their tracing of the matter field. Conversely, galaxy clustering measurements depend only on μ and are insensitive to Σ (Abbott et al. 2019). Constraints on (μ, Σ), or similar quantities but with different names, are already very good (Hojjati et al. 2016; Salvatelli et al. 2016; Mueller et al. 2018; Abbott et al. 2019). More ambitious analyses promote μ and Σ to few-parameter functions of redshift (Daniel and Linder 2013; Simpson 2013; Ade et al. 2016; Aghanim et al. 2020; Abbott et al. 2019, 2023a). Comparison of $\mu(a)$ and $\Sigma(a)$ to their fiducial values of zero thus constitutes a test of modified gravity.

5 Conclusions

We have described how the growth of structure determines key aspects of observable quantities in cosmology, such as the spatial correlation of galaxies, the coherence of their peculiar velocities, the amplitude and spatial dependence of cosmic shear, the abundance of galaxy clusters, and lensing of the cosmic microwave background (CMB) photons. Observations of these quantities can provide important constraints on growth, which in turn helps constrain cosmological models, and specifically distinguishes between dark energy and modified gravity.

Notably, current constraints on the amplitude of mass fluctuations S_8 and the function $f\sigma_8$ come largely from growth. They can be used to look for consistency of data with a cosmological model, as the S_8 and $f\sigma_8(z)$ constraints are model dependent. These constraints can also be used to look for internal consistency between different probes or datasets, as well as comparison between early- and late-universe constraints. Such comparisons have been very fruitful, and have led to the currently much-discussed S_8 tension, where the CMB experiments appear to give a higher value of this quantity than cosmic-shear measurements.

We highlighted several ways in which growth can be used to probe the cosmological model that go beyond simply measuring and reporting σ_8, S_8 or $f\sigma_8(z)$. Explicit parameterization of the growth sector is one such approach. For example, departures from growth predicted assuming general relativity can be enabled by freeing the growth index γ from its general-relativistic value of $\simeq 0.55$, or by

parameterizing the deviations of gravitational potentials Ψ and Φ from their fiducial values. One can also encode additional freedom in the linear growth function $D(a)$ as a function of scale or time. Alternatively, one can explicitly separate information contained in the growth of structure from that in geometrical terms by introducing separate geometry and growth parameters in equations that govern cosmological observables. Because relations between the geometrical and growth quantities that are obeyed in LCDM and wCDM are likely to be broken in modified-gravity explanations of the accelerating universe, such "geometry-growth split" tests are potentially very powerful. Finally, we discussed how simply making predictions given by measurements by one set of probes (e.g., the CMB) for what another set of measurements (e.g., cosmic shear or some other, new probe, or an existing probe in a new range of scales or redshifts) is expected to measure, is also a very useful way to employ growth to stress-test the cosmological model.

Most of the major upcoming experiments and telescopes with the role to probe the accelerating universe rely on better measurements of growth, particularly at higher redshifts ($z \simeq 2$-5) than currently possible, in order to better understand dark energy and dark matter (see Annis et al. 2022 for a recent review). Therefore, we expect that the measurements and interpretations of the growth of structure will become even more central to cosmology in the years to come.

Acknowledgements I would like to thank Eric Linder and GongBo Zhao for helpful comments on the manuscript. Over the couple of years over which this manuscript evolved, my work has been supported by NASA under contract 19-ATP19-0058, DOE under Contract No. DE-FG02-95ER40899, NSF under contract AST-1812961, and Leinweber Center for Theoretical Physics at the University of Michigan. I would also like to thank Aspen Center for Physics and Max Planck Institute for Astrophysics for their hospitality.

References

Abbott TMC et al (2019) Dark Energy Survey Year 1 results: constraints on extended cosmological models from galaxy clustering and weak lensing. Phys Rev D 99(12):123505. https://doi.org/10.1103/PhysRevD.99.123505. arXiv:1810.02499 [astro-ph.CO]

Abbott TMC et al (2020) Dark Energy Survey Year 1 results: cosmological constraints from cluster abundances and weak lensing. Phys Rev D 102(2):023509. https://doi.org/10.1103/PhysRevD.102.023509. arXiv:2002.11124 [astro-ph.CO]

Abbott TMC et al (2022) Dark Energy Survey Year 3 results: cosmological constraints from galaxy clustering and weak lensing. Phys Rev D 105(2):023520. https://doi.org/10.1103/PhysRevD.105.023520. arXiv:2105.13549 [astro-ph.CO]

Abbott TMC et al (2023) Dark Energy Survey Year 3 results: constraints on extensions to ΛCDM with weak lensing and galaxy clustering. Phys Rev D 107(8):083504. https://doi.org/10.1103/PhysRevD.107.083504. arXiv:2207.05766 [astro-ph.CO]

Abbott TMC et al (2023) Joint analysis of Dark Energy Survey Year 3 data and CMB lensing from SPT and Planck. III. Combined cosmological constraints. Phys Rev D 107(2):023531. https://doi.org/10.1103/PhysRevD.107.023531. arXiv:2206.10824 [astro-ph.CO]

Abramo LR, Bertacca D (2017) Disentangling the effects of Doppler velocity and primordial non-Gaussianity in galaxy power spectra. Phys Rev D 96(12):123535. https://doi.org/10.1103/PhysRevD.96.123535. arXiv:1706.01834 [astro-ph.CO]

Ade PAR et al (2016) Planck 2015 results. XIV. Dark energy and modified gravity. Astron Astrophys 594:A14. https://doi.org/10.1051/0004-6361/201525814. arXiv:1502.01590 [astro-ph.CO]

Aghanim N et al (2020) Planck 2018 results. VI. Cosmological parameters. Astron Astrophys 641:A6. https://doi.org/10.1051/0004-6361/201833910, [Erratum: Astron Astrophys 652:C4 (2021)]. arXiv:1807.06209 [astro-ph.CO]

Aiola S et al (2020) The Atacama Cosmology Telescope: DR4 Maps and cosmological parameters. JCAP 12:047. https://doi.org/10.1088/1475-7516/2020/12/047. arXiv:2007.07288 [astro-ph.CO]

Alam S et al (2021) Completed SDSS-IV extended Baryon oscillation spectroscopic survey: cosmological implications from two decades of spectroscopic surveys at the Apache Point Observatory. Phys Rev D 103(8):083533. https://doi.org/10.1103/PhysRevD.103.083533. arXiv:2007.08991 [astro-ph.CO]

Allen SW, Evrard AE, Mantz AB (2011) Cosmological Parameters from Observations of Galaxy Clusters. Annu Rev Astron Astrophys 49:409–470. https://doi.org/10.1146/annurev-astro-081710-102514. arXiv:1103.4829 [astro-ph.CO]

Alonso D, Ferreira PG (2015) Constraining ultralarge-scale cosmology with multiple tracers in optical and radio surveys. Phys Rev D 92(6):063525. https://doi.org/10.1103/PhysRevD.92.063525. arXiv:1507.03550 [astro-ph.CO]

Alonso D, Bull P, Ferreira PG et al (2015) Ultra large-scale cosmology in next-generation experiments with single tracers. Astrophys J 814(2):145. https://doi.org/10.1088/0004-637X/814/2/145. arXiv:1505.07596 [astro-ph.CO]

Amendola L, Kunz M, Sapone D (2008) Measuring the dark side (with weak lensing). JCAP 04:013. https://doi.org/10.1088/1475-7516/2008/04/013. arXiv:0704.2421 [astro-ph]

Amendola L, Fogli S, Guarnizo A et al (2014) Model-independent constraints on the cosmological anisotropic stress. Phys Rev D 89(6):063538. https://doi.org/10.1103/PhysRevD.89.063538. arXiv:1311.4765 [astro-ph.CO]

Amon A et al (2022) Dark Energy Survey Year 3 results: cosmology from cosmic shear and robustness to data calibration. Phys Rev D 105(2):023514. https://doi.org/10.1103/PhysRevD.105.023514. arXiv:2105.13543 [astro-ph.CO]

Andrade U, Anbajagane D, von Marttens R et al (2021) A test of the standard cosmological model with geometry and growth. JCAP 11:014. https://doi.org/10.1088/1475-7516/2021/11/014. arXiv:2107.07538 [astro-ph.CO]

Annis J, Newman JA, Slosar A (2022) Snowmass2021 Cosmic Frontier: Report of the CF04 Topical Group on Dark Energy and Cosmic Acceleration in the Modern Universe. arXiv e-prints arXiv:2209.08049 [astro-ph.CO]

Asgari M et al (2021) KiDS-1000 cosmology: cosmic shear constraints and comparison between two point statistics. Astron Astrophys 645:A104. https://doi.org/10.1051/0004-6361/202039070. arXiv:2007.15633 [astro-ph.CO]

Bahcall NA, Fan Xh (1998) The most massive distant clusters: determining Ω and σ_8. Astrophys J 504:1. https://doi.org/10.1086/306088. arXiv:astro-ph/9803277

Baker T, Ferreira PG, Skordis C et al (2011) Towards a fully consistent parameterization of modified gravity. Phys Rev D 84:124018. https://doi.org/10.1103/PhysRevD.84.124018. arXiv:1107.0491 [astro-ph.CO]

Baker T, Ferreira PG, Skordis C (2013) The Parameterized Post-Friedmann framework for theories of modified gravity: concepts, formalism and examples. Phys Rev D 87(2):024015. https://doi.org/10.1103/PhysRevD.87.024015. arXiv:1209.2117 [astro-ph.CO]

Baldi M, Pettorino V, Robbers G et al (2010) Hydrodynamical N-body simulations of coupled dark energy cosmologies. Mon Not R Astron Soc 403:1684–1702. https://doi.org/10.1111/j.1365-2966.2009.15987.x. arXiv:0812.3901 [astro-ph]

Barreira A (2022) Can we actually constrain f_{NL} using the scale-dependent bias effect? An illustration of the impact of galaxy bias uncertainties using the BOSS DR12 galaxy power spectrum. JCAP 11:013. https://doi.org/10.1088/1475-7516/2022/11/013. arXiv:2205.05673 [astro-ph.CO]

Barreira A, Li B, Hellwing WA et al (2014) Nonlinear structure formation in Nonlocal Gravity. JCAP 09:031. https://doi.org/10.1088/1475-7516/2014/09/031. arXiv:1408.1084 [astro-ph.CO]

Bartelmann M, Schneider P (2001) Phys Rept 340:291–472. https://doi.org/10.1016/S0370-1573(00)00082-X. arXiv:astro-ph/9912508

Battye RA, Pearson JA (2012) Effective action approach to cosmological perturbations in dark energy and modified gravity. JCAP 1207:019. https://doi.org/10.1088/1475-7516/2012/07/019. arXiv:1203.0398 [hep-th]

Bernal JL, Verde L, Cuesta AJ (2016) Parameter splitting in dark energy: is dark energy the same in the background and in the cosmic structures? JCAP 02:059. https://doi.org/10.1088/1475-7516/2016/02/059. arXiv:1511.03049 [astro-ph.CO]

Bernstein GM, Jain B (2004) Dark energy constraints from weak-lensing cross-correlation cosmography. Astrophys J 600:17–25. https://doi.org/10.1086/379768. arXiv:astro-ph/0309332
Bertschinger E (2006) On the growth of perturbations as a test of dark energy. Astrophys J 648:797–806. https://doi.org/10.1086/506021. arXiv:astro-ph/0604485
Beutler F, Blake C, Colless M et al (2012) The 6dF Galaxy Survey: $z \approx 0$ measurement of the growth rate and $_8$. Mon Not R Astron Soc 423:3430–3444. https://doi.org/10.1111/j.1365-2966.2012.21136.x. arXiv:1204.4725 [astro-ph.CO]
Bird S, Ali-Haïmoud Y, Feng Y et al (2018) An efficient and accurate hybrid method for simulating non-linear neutrino structure. Mon Not R Astron Soc 481(2):1486–1500. https://doi.org/10.1093/mnras/sty2376. arXiv:1803.09854 [astro-ph.CO]
Blake C et al (2012) The WiggleZ Dark Energy Survey: joint measurements of the expansion and growth history at $z<1$. Mon Not R Astron Soc 425:405–414. https://doi.org/10.1111/j.1365-2966.2012.21473.x. arXiv:1204.3674 [astro-ph.CO]
Blake C et al (2013) Galaxy And Mass Assembly (GAMA): improved cosmic growth measurements using multiple tracers of large-scale structure. Mon Not R Astron Soc 436:3089. https://doi.org/10.1093/mnras/stt1791. arXiv:1309.5556 [astro-ph.CO]
Bloomfield JK, Flanagan EE, Park M et al (2013) Dark energy or modified gravity? An effective field theory approach. JCAP 1308:010. https://doi.org/10.1088/1475-7516/2013/08/010. arXiv:1211.7054 [astro-ph.CO]
Bocquet S, Heitmann K, Habib S et al (2020) The Mira-Titan Universe. III. Emulation of the Halo Mass Function. Astrophys J 901(1):5. https://doi.org/10.3847/1538-4357/abac5c. arXiv:2003.12116 [astro-ph.CO]
Bocquet S et al (2019) Cluster cosmology constraints from the 2500 deg^2 SPT-SZ survey: inclusion of weak gravitational lLensing data from Magellan and the Hubble Space Telescope. Astrophys J 878 (1):55. https://doi.org/10.3847/1538-4357/ab1f10. arXiv:1812.01679 [astro-ph.CO]
Bond JR, Cole S, Efstathiou G et al (1991) Excursion set mass functions for hierarchical Gaussian fluctuations. Astrophys J 379:440. https://doi.org/10.1086/170520
Bonvin C (2014) Isolating relativistic effects in large-scale structure. Class Quant Grav 31(23):234002. https://doi.org/10.1088/0264-9381/31/23/234002. arXiv:1409.2224 [astro-ph.CO]
Boruah SS, Hudson MJ, Lavaux G (2020) Cosmic flows in the nearby universe: new peculiar velocities from SNe and cosmological constraints. Mon Not R Astron Soc 498(2):2703–2718. https://doi.org/10.1093/mnras/staa2485. arXiv:1912.09383 [astro-ph.CO]
Bose S, Li B, Barreira A et al (2017) Speeding up N-body simulations of modified gravity: Chameleon screening models. JCAP 02:050. https://doi.org/10.1088/1475-7516/2017/02/050. arXiv:1611.09375 [astro-ph.CO]
Brodwin M et al (2010) SPT-CL J0546–5345: a massive $z > 1$ galaxy cluster selected via the Sunyaev-Zel'dovich effect with the South Pole Telescope. Astrophys J 721:90–97. https://doi.org/10.1088/0004-637X/721/1/90. arXiv:1006.5639
Caldwell R, Cooray A, Melchiorri A (2007) Constraints on a new post-general relativity cosmological parameter. Phys Rev D 76:023507. https://doi.org/10.1103/PhysRevD.76.023507. arXiv:astro-ph/0703375 [ASTRO-PH]
Casarini L, Bonometto SA, Tessarotto E et al (2016) Extending the Coyote emulator to dark energy models with standard w_0-w_a parametrization of the equation of state. JCAP 08:008. https://doi.org/10.1088/1475-7516/2016/08/008. arXiv:1601.07230 [astro-ph.CO]
Catelan P, Kamionkowski M, Blandford RD (2001) Intrinsic and extrinsic galaxy alignment. Mon Not R Astron Soc 320:L7–L13. https://doi.org/10.1046/j.1365-8711.2001.04105.x. arXiv:astro-ph/0005470
Challinor A, Lewis A (2011) The linear power spectrum of observed source number counts. Phys Rev D 84:043516. https://doi.org/10.1103/PhysRevD.84.043516. arXiv:1105.5292 [astro-ph.CO]
Chan KC, Scoccimarro R (2009) Large-scale structure in brane-induced gravity II. Numerical simulations. Phys Rev D 80:104005. https://doi.org/10.1103/PhysRevD.80.104005. arXiv:0906.4548 [astro-ph.CO]
Chen SF, White M, DeRose J et al (2022) Cosmological analysis of three-dimensional BOSS galaxy clustering and Planck CMB lensing cross correlations via Lagrangian perturbation theory. JCAP 07 (07):041. https://doi.org/10.1088/1475-7516/2022/07/041. arXiv:2204.10392 [astro-ph.CO]
Creminelli P, D'Amico G, Norena J et al (2009) The effective theory of quintessence: the $w< -1$ Side Unveiled. JCAP 0902:018. https://doi.org/10.1088/1475-7516/2009/02/018. arXiv:0811.0827 [astro-ph]

Dalal R, et al (2023) Hyper Suprime-Cam Year 3 Results: Cosmology from cosmic shear power spectra. arXiv e-prints arXiv:2304.00701 [astro-ph.CO]
Daniel SF, Linder EV (2010) Confronting general relativity with further cosmological data. Phys Rev D 82:103523. https://doi.org/10.1103/PhysRevD.82.103523. arXiv:1008.0397 [astro-ph.CO]
Daniel SF, Linder EV (2013) Constraining cosmic expansion and gravity with galaxy redshift surveys. JCAP 1302:007. https://doi.org/10.1088/1475-7516/2013/02/007. arXiv:1212.0009 [astro-ph.CO]
DeRose J, Wechsler RH, Tinker JL et al (2019) The Aemulus Project I: numerical simulations for precision cosmology. Astrophys J 875(1):69. https://doi.org/10.3847/1538-4357/ab1085. arXiv:1804.05865 [astro-ph.CO]
Dvali GR, Gabadadze G, Porrati M (2000) 4-D gravity on a brane in 5-D Minkowski space. Phys Lett B 485:208–214. https://doi.org/10.1016/S0370-2693(00)00669-9. arXiv:hep-th/0005016
Fonseca J, Camera S, Santos M et al (2015) Hunting down horizon-scale effects with multi-wavelength surveys. Astrophys J Lett 812(2):L22. https://doi.org/10.1088/2041-8205/812/2/L22. arXiv:1507.04605 [astro-ph.CO]
Francis MJ, Lewis GF, Linder EV (2007) Power spectra to 1% accuracy between dynamical dark energy cosmologies. Mon Not R Astron Soc 380:1079. https://doi.org/10.1111/j.1365-2966.2007.12139.x. arXiv:0704.0312 [astro-ph]
García-García C, Zapatero JR, Alonso D et al (2021) The growth of density perturbations in the last ~ 10 billion years from tomographic large-scale structure data. JCAP 10:030. https://doi.org/10.1088/1475-7516/2021/10/030. arXiv:2105.12108 [astro-ph.CO]
Garrison LH, Eisenstein DJ, Ferrer D et al (2018) The Abacus Cosmos: a suite of cosmological N-body simulations. Astrophys J Suppl 236(2):43. https://doi.org/10.3847/1538-4365/aabfd3. arXiv:1712.05768 [astro-ph.CO]
Gleyzes J, Langlois D, Piazza F et al (2013) Essential building blocks of dark energy. JCAP 1308:025. https://doi.org/10.1088/1475-7516/2013/08/025. arXiv:1304.4840 [hep-th]
Gleyzes J, Langlois D, Piazza F et al (2015) Exploring gravitational theories beyond Horndeski. JCAP 1502:018. https://doi.org/10.1088/1475-7516/2015/02/018. arXiv:1408.1952 [astro-ph.CO]
Grimm N, Scaccabarozzi F, Yoo J et al (2020) Galaxy power spectrum in general relativity. JCAP 11:064. https://doi.org/10.1088/1475-7516/2020/11/064. arXiv:2005.06484 [astro-ph.CO]
Haiman Z, Mohr JJ, Holder GP (2000) Constraints on quintessence from future galaxy cluster surveys. Astrophys J 553:545. https://doi.org/10.1086/320939. arXiv:astro-ph/0002336
Hamilton AJS, Matthews A, Kumar P et al (1991) Reconstructing the primordial spectrum of fluctuations of the universe from the observed nonlinear clustering of galaxies. Astrophys J Lett 374:L1. https://doi.org/10.1086/186057
Hand N et al (2012) Evidence of Galaxy cluster motions with the kinematic Sunyaev-Zel'dovich effect. Phys Rev Lett 109:041101. https://doi.org/10.1103/PhysRevLett.109.041101. arXiv:1203.4219 [astro-ph.CO]
Heitmann K, Higdon D, White M et al (2009) The coyote universe II: cosmological models and precision emulation of the nonlinear matter power spectrum. Astrophys J 705:156–174. https://doi.org/10.1088/0004-637X/705/1/156. arXiv:0902.0429 [astro-ph.CO]
Heitmann K, Lawrence E, Kwan J et al (2014) The coyote universe extended: precision emulation of the matter power spectrum. Astrophys J 780:111. https://doi.org/10.1088/0004-637X/780/1/111. arXiv:1304.7849 [astro-ph.CO]
Heymans C et al (2021) KiDS-1000 cosmology: Multi-probe weak gravitational lensing and spectroscopic galaxy clustering constraints. Astron Astrophys 646:A140. https://doi.org/10.1051/0004-6361/202039063. arXiv:2007.15632 [astro-ph.CO]
Hikage C et al (2019) Cosmology from cosmic shear power spectra with Subaru Hyper Suprime-Cam first-year data. Publ Astron Soc Jap 71(2):43. https://doi.org/10.1093/pasj/psz010. arXiv:1809.09148 [astro-ph.CO]
Hirata CM, Seljak U (2004) Intrinsic alignment-lensing interference as a contaminant of cosmic shear. Phys Rev D 70:063526. https://doi.org/10.1103/PhysRevD.82.049901, [Erratum: Phys Rev D 82:049901 (2010)]. arXiv:astro-ph/0406275
Hoekstra H, Jain B (2008) Weak gravitational lensing and its cosmological applications. Annu Rev Nucl Part Sci 58:99–123. https://doi.org/10.1146/annurev.nucl.58.110707.171151. arXiv:0805.0139 [astro-ph]
Hojjati A, Pogosian L, Silvestri A et al (2014) Observable physical modes of modified gravity. Phys Rev D 89(8):083505. https://doi.org/10.1103/PhysRevD.89.083505. arXiv:1312.5309 [astro-ph.CO]

Hojjati A, Plahn A, Zucca A et al (2016) Searching for scalar gravitational interactions in current and future cosmological data. Phys Rev D 93(4):043531. https://doi.org/10.1103/PhysRevD.93.043531. arXiv:1511.05962 [astro-ph.CO]

Holz DE, Perlmutter S (2012) The most massive objects in the Universe. Astrophys J Lett 755:L36. https://doi.org/10.1088/2041-8205/755/2/L36. arXiv:1004.5349 [astro-ph.CO]

Howlett C, Ross A, Samushia L et al (2015) The clustering of the SDSS main galaxy sample – II. Mock galaxy catalogues and a measurement of the growth of structure from redshift space distortions at $z = 0.15$. Mon Not R Astron Soc 449(1):848–866. https://doi.org/10.1093/mnras/stu2693. arXiv:1409.3238 [astro-ph.CO]

Howlett C, Said K, Lucey JR et al (2022) The Sloan Digital Sky Survey peculiar velocity catalogue. Mon Not R Astron Soc 515(1):953–976. https://doi.org/10.1093/mnras/stac1681. arXiv:2201.03112 [astro-ph.CO]

Hu W (2002) Dark energy and matter evolution from lensing tomography. Phys Rev D 66:083515. https://doi.org/10.1103/PhysRevD.66.083515. arXiv:astro-ph/0208093

Hu W, Sawicki I (2007) A parameterized post-friedmann framework for modified gravity. Phys Rev D 76:104043. https://doi.org/10.1103/PhysRevD.76.104043. arXiv:0708.1190 [astro-ph]

Huterer D (2023) A Course in Cosmology: From Theory to Practice. Cambridge University Press, Cambridge, https://doi.org/10.1017/9781009070232

Huterer D, Linder EV (2007) Separating dark physics from physical darkness: Minimalist modified gravity versus dark energy. Phys Rev D 75:023519. https://doi.org/10.1103/PhysRevD.75.023519. arXiv:astro-ph/0608681

Huterer D, Shafer D, Scolnic D et al (2017) Testing ΛCDM at the lowest redshifts with SN Ia and galaxy velocities. JCAP 05:015. https://doi.org/10.1088/1475-7516/2017/05/015. arXiv:1611.09862 [astro-ph.CO]

Huterer D et al (2015) Growth of cosmic structure: probing dark energy beyond expansion. Astropart Phys 63:23–41. https://doi.org/10.1016/j.astropartphys.2014.07.004. arXiv:1309.5385 [astro-ph.CO]

Ishak M, Upadhye A, Spergel DN (2006) Probing cosmic acceleration beyond the equation of state: distinguishing between dark energy and modified gravity models. Phys Rev D 74:043513. https://doi.org/10.1103/PhysRevD.74.043513. arXiv:astro-ph/0507184

Jee MJ, Hughes JP, Menanteau F, et al (2014) Weighing "El Gordo" with a precision scale: Hubble Space Telescope weak-lensing analysis of the merging galaxy cluster ACT-CL J0102–4915 at $z = 0.87$. Astrophys J 785:20. https://doi.org/10.1088/0004-637X/785/1/20, arXiv:1309.5097 [astro-ph.CO]

Jeong D, Schmidt F, Hirata CM (2012) Large-scale clustering of galaxies in general relativity. Phys Rev D 85:023504. https://doi.org/10.1103/PhysRevD.85.023504. arXiv:1107.5427 [astro-ph.CO]

Knabenhans M et al (2021) Euclid preparation: IX. EuclidEmulator2—power spectrum emulation with massive neutrinos and self-consistent dark energy perturbations. Mon Not R Astron Soc 505 (2):2840–2869. https://doi.org/10.1093/mnras/stab1366. arXiv:2010.11288 [astro-ph.CO]

Knox L, Song YS, Tyson JA (2006) Distance-redshift and growth-redshift relations as two windows on acceleration and gravitation: Dark energy or new gravity? Phys Rev D 74:023512. https://doi.org/10.1103/PhysRevD.74.023512. arXiv:astro-ph/0503644

Kobayashi Y, Nishimichi T, Takada M et al (2022) Full-shape cosmology analysis of the SDSS-III BOSS galaxy power spectrum using an emulator-based halo model: A 5% determination of σ_8. Phys Rev D 105(8):083517. https://doi.org/10.1103/PhysRevD.105.083517. arXiv:2110.06969 [astro-ph.CO]

Koyama K, Taruya A, Hiramatsu T (2009) Non-linear evolution of matter power spectrum in modified theory of gravity. Phys Rev D 79:123512. https://doi.org/10.1103/PhysRevD.79.123512. arXiv:0902.0618 [astro-ph.CO]

Kravtsov A, Borgani S (2012) Formation of galaxy clusters. Annu Rev Astron Astrophys 50:353–409. https://doi.org/10.1146/annurev-astro-081811-125502. arXiv:1205.5556 [astro-ph.CO]

Krolewski A, Ferraro S, Schlafly EF et al (2020) unWISE tomography of Planck CMB lensing. JCAP 05:047. https://doi.org/10.1088/1475-7516/2020/05/047. arXiv:1909.07412 [astro-ph.CO]

Krolewski A, Ferraro S, White M (2021) Cosmological constraints from unWISE and Planck CMB lensing tomography. JCAP 12(12):028. https://doi.org/10.1088/1475-7516/2021/12/028. arXiv:2105.03421 [astro-ph.CO]

Laszlo I, Bean R (2008) Nonlinear growth in modified gravity theories of dark energy. Phys Rev D 77:024048. https://doi.org/10.1103/PhysRevD.77.024048. arXiv:0709.0307 [astro-ph]

Lawrence E, Heitmann K, Kwan J et al (2017) The Mira-Titan Universe II: matter power spectrum emulation. Astrophys J 847(1):50. https://doi.org/10.3847/1538-4357/aa86a9. arXiv:1705.03388 [astro-ph.CO]

Lesgourgues J, Pastor S (2006) Massive neutrinos and cosmology. Phys Rept 429:307–379. https://doi.org/10.1016/j.physrep.2006.04.001. arXiv:astro-ph/0603494
Li B, Barreira A, Baugh CM et al (2013) Simulating the quartic Galileon gravity model on adaptively refined meshes. JCAP 11:012. https://doi.org/10.1088/1475-7516/2013/11/012. arXiv:1308.3491 [astro-ph.CO]
Li X, et al (2023) Hyper Suprime-Cam Year 3 Results: Cosmology from Cosmic Shear Two-point Correlation Functions. arXiv e-prints arXiv:2304.00702 [astro-ph.CO]
Linder EV (2005) Cosmic growth history and expansion history. Phys Rev D 72:043529. https://doi.org/10.1103/PhysRevD.72.043529. arXiv:astro-ph/0507263
Linder EV, Cahn RN (2007) Parameterized Beyond-Einstein Growth. Astropart Phys 28:481–488. https://doi.org/10.1016/j.astropartphys.2007.09.003. arXiv:astro-ph/0701317
Linder EV, Jenkins A (2003) Cosmic structure and dark energy. Mon Not R Astron Soc 346:573. https://doi.org/10.1046/j.1365-2966.2003.07112.x. arXiv:astro-ph/0305286
Lue A, Scoccimarro R, Starkman G (2004) Differentiating between modified gravity and dark energy. Phys Rev D 69:044005. https://doi.org/10.1103/PhysRevD.69.044005. arXiv:astro-ph/0307034
Maartens R, Zhao GB, Bacon D et al (2013) Relativistic corrections and non-Gaussianity in radio continuum surveys. JCAP 02:044. https://doi.org/10.1088/1475-7516/2013/02/044. arXiv:1206.0732 [astro-ph.CO]
Mandelbaum R (2018) Weak lensing for precision cosmology. Annu Rev Astron Astrophys 56:393–433. https://doi.org/10.1146/annurev-astro-081817-051928. arXiv:1710.03235 [astro-ph.CO]
McClintock T, Rozo E, Becker MR et al (2019) The Aemulus project II: emulating the Halo mass function. Astrophys J 872(1):53. https://doi.org/10.3847/1538-4357/aaf568. arXiv:1804.05866 [astro-ph.CO]
Mead A, Peacock J, Heymans C et al (2015) An accurate halo model for fitting non-linear cosmological power spectra and baryonic feedback models. Mon Not R Astron Soc 454(2):1958–1975. https://doi.org/10.1093/mnras/stv2036. arXiv:1505.07833 [astro-ph.CO]
Mead A, Brieden S, Tröster T, et al (2020) HMcode-2020: Improved modelling of non-linear cosmological power spectra with baryonic feedback. Mon Not R Astron Soc https://doi.org/10.1093/mnras/stab082, arXiv:2009.01858 [astro-ph.CO]
Miranda V, Dvorkin C (2018) Model-independent predictions for smooth cosmic acceleration scenarios. Phys Rev D 98(4):043537. https://doi.org/10.1103/PhysRevD.98.043537. arXiv:1712.04289 [astro-ph.CO]
Mo H, van den Bosch FC, White S (2010) Galaxy Formation and Evolution. Cambridge University Press, Cambridge, UK, https://doi.org/10.1017/CBO9780511807244
Mortonson MJ, Hu W, Huterer D (2009) Falsifying paradigms for cosmic acceleration. Phys Rev D 79:023004. https://doi.org/10.1103/PhysRevD.79.023004. arXiv:0810.1744 [astro-ph]
Mortonson MJ, Hu W, Huterer D (2010) Testable dark energy predictions from current data. Phys Rev D 81:063007. https://doi.org/10.1103/PhysRevD.81.063007. arXiv:0912.3816 [astro-ph.CO]
Mortonson MJ, Hu W, Huterer D (2011) Simultaneous Falsification of ΛCDM and quintessence with massive. Distant Clusters. Phys Rev D 83:023015. https://doi.org/10.1103/PhysRevD.83.023015. arXiv:1011.0004 [astro-ph.CO]
Mueller EM, Percival W, Linder E et al (2018) The clustering of galaxies in the completed SDSS-III Baryon Oscillation Spectroscopic Survey: constraining modified gravity. Mon Not R Astron Soc 475 (2):2122–2131. https://doi.org/10.1093/mnras/stx3232. arXiv:1612.00812 [astro-ph.CO]
Muir J et al (2021) DES Y1 results: splitting growth and geometry to test ΛCDM. Phys Rev D 103 (2):023528. https://doi.org/10.1103/PhysRevD.103.023528. arXiv:2010.05924 [astro-ph.CO]
Mullis CR et al (2005) Discovery of an X-ray-Luminous Galaxy Cluster at $z = 1.4$. Astrophys J 623:L85–L88. https://doi.org/10.1086/429801. arXiv:astro-ph/0503004
Newman JA, Gruen D (2022) Photometric redshifts for next-generation surveys. Annu Rev Astron Astrophys https://doi.org/10.1146/annurev-astro-032122-014611, arXiv:2206.13633 [astro-ph.CO]
Nishimichi T et al (2019) Dark Quest. I. Fast and accurate emulation of Halo clustering statistics and its application to Galaxy clustering. Astrophys J 884:29. https://doi.org/10.3847/1538-4357/ab3719. arXiv:1811.09504 [astro-ph.CO]
Noller J, von Braun-Bates F, Ferreira PG (2014) Relativistic scalar fields and the quasistatic approximation in theories of modified gravity. Phys Rev D 89(2):023521. https://doi.org/10.1103/PhysRevD.89.023521. arXiv:1310.3266 [astro-ph.CO]
Okumura T, et al (2016) The Subaru FMOS galaxy redshift survey (FastSound). IV. New constraint on gravity theory from redshift space distortions at $z \sim 1.4$. Publ Astron Soc Jap 68(3):38. https://doi.org/10.1093/pasj/psw029, arXiv:1511.08083 [astro-ph.CO]

Oyaizu H, Lima M, Hu W (2008) Nonlinear evolution of f(R) cosmologies. 2. Power spectrum. Phys Rev D 78:123524. https://doi.org/10.1103/PhysRevD.78.123524. arXiv:0807.2462 [astro-ph]
Peacock JA, Bilicki M (2018) Wide-area tomography of CMB lensing and the growth of cosmological density fluctuations. Mon Not R Astron Soc 481(1):1133–1148. https://doi.org/10.1093/mnras/sty2314. arXiv:1805.11525 [astro-ph.CO]
Peacock JA, Dodds SJ (1996) Nonlinear evolution of cosmological power spectra. Mon Not R Astron Soc 280:L19. https://doi.org/10.1093/mnras/280.3.L19. arXiv:astro-ph/9603031
Peebles PJE (1994) Principles of physical cosmology. Princeton University Press, Princeton
Pezzotta A, et al (2017) The VIMOS Public Extragalactic Redshift Survey (VIPERS): The growth of structure at $0.5<z<1.2$ from redshift-space distortions in the clustering of the PDR-2 final sample. Astron Astrophys 604:A33. https://doi.org/10.1051/0004-6361/201630295, arXiv:1612.05645 [astro-ph.CO]
Philcox OHE, Ivanov MM (2022) BOSS DR12 full-shape cosmology: ΛCDM constraints from the large-scale galaxy power spectrum and bispectrum monopole. Phys Rev D 105(4):043517. https://doi.org/10.1103/PhysRevD.105.043517. arXiv:2112.04515 [astro-ph.CO]
Press WH, Schechter P (1974) Formation of galaxies and clusters of galaxies by selfsimilar gravitational condensation. Astrophys J 187:425–438. https://doi.org/10.1086/152650
Raveri M (2020) Reconstructing gravity on cosmological scales. Phys Rev D 101(8):083524. https://doi.org/10.1103/PhysRevD.101.083524. arXiv:1902.01366 [astro-ph.CO]
Ruiz EJ, Huterer D (2015) Testing the dark energy consistency with geometry and growth. Phys Rev D 91:063009. https://doi.org/10.1103/PhysRevD.91.063009. arXiv:1410.5832 [astro-ph.CO]
Ruiz-Zapatero J et al (2021) Geometry versus growth—internal consistency of the flat ΛCDM model with KiDS-1000. Astron Astrophys 655:A11. https://doi.org/10.1051/0004-6361/202141350. arXiv:2105.09545 [astro-ph.CO]
Said K, Colless M, Magoulas C et al (2020) Joint analysis of 6dFGS and SDSS peculiar velocities for the growth rate of cosmic structure and tests of gravity. Mon Not R Astron Soc 497(1):1275–1293. https://doi.org/10.1093/mnras/staa2032. arXiv:2007.04993 [astro-ph.CO]
Salvatelli V, Piazza F, Marinoni C (2016) Constraints on modified gravity from Planck 2015: when the health of your theory makes the difference. JCAP 1609(09):027. https://doi.org/10.1088/1475-7516/2016/09/027. arXiv:1602.08283 [astro-ph.CO]
Schmidt F (2009) Self-consistent cosmological simulations of DGP braneworld gravity. Phys Rev D 80:043001. https://doi.org/10.1103/PhysRevD.80.043001. arXiv:0905.0858 [astro-ph.CO]
Secco LF et al (2022) Dark energy survey year 3 results: cosmology from cosmic shear and robustness to modeling uncertainty. Phys Rev D 105(2):023515. https://doi.org/10.1103/PhysRevD.105.023515. arXiv:2105.13544 [astro-ph.CO]
Silvestri A, Pogosian L, Buniy RV (2013) Practical approach to cosmological perturbations in modified gravity. Phys Rev D 87(10):104015. https://doi.org/10.1103/PhysRevD.87.104015. arXiv:1302.1193 [astro-ph.CO]
Simpson F et al (2013) CFHTLenS: testing the laws of gravity with tomographic weak lensing and redshift space distortions. Mon Not R Astron Soc 429:2249. https://doi.org/10.1093/mnras/sts493. arXiv:1212.3339 [astro-ph.CO]
Smith RE, Peacock JA, Jenkins A et al (2003) Stable clustering, the halo model and nonlinear cosmological power spectra. Mon Not R Astron Soc 341:1311. https://doi.org/10.1046/j.1365-8711.2003.06503.x. arXiv:astro-ph/0207664
Song YS, Percival WJ (2009) Reconstructing the history of structure formation using redshift distortions. JCAP 10:004. https://doi.org/10.1088/1475-7516/2009/10/004. arXiv:0807.0810 [astro-ph]
Song YS, Zhao GB, Bacon D et al (2011) Complementarity of weak lensing and peculiar velocity measurements in testing general relativity. Phys Rev D 84:083523. https://doi.org/10.1103/PhysRevD.84.083523. arXiv:1011.2106 [astro-ph.CO]
Stabenau HF, Jain B (2006) N-body simulations of alternate gravity models. Phys Rev D 74:084007. https://doi.org/10.1103/PhysRevD.74.084007. arXiv:astro-ph/0604038
Sugiyama S, et al (2023) Hyper Suprime-Cam Year 3 Results: Cosmology from Galaxy Clustering and Weak Lensing with HSC and SDSS using the Minimal Bias Model. arXiv e-prints arXiv:2304.00705 [astro-ph.CO]
Takahashi R, Sato M, Nishimichi T et al (2012) Revising the Halofit model for the nonlinear matter power spectrum. Astrophys J 761:152. https://doi.org/10.1088/0004-637X/761/2/152. arXiv:1208.2701 [astro-ph.CO]

Tansella V, Bonvin C, Durrer R et al (2018) The full-sky relativistic correlation function and power spectrum of galaxy number counts. Part I: theoretical aspects. JCAP 03:019. https://doi.org/10.1088/1475-7516/2018/03/019. arXiv:1708.00492 [astro-ph.CO]

Tinker JL, Kravtsov AV, Klypin A et al (2008) Toward a halo mass function for precision cosmology: the limits of universality. Astrophys J 688:709–728. https://doi.org/10.1086/591439. arXiv:0803.2706 [astro-ph]

de la Torre S, Guzzo L (2012) Modelling non-linear redshift-space distortions in the galaxy clustering pattern: systematic errors on the growth rate parameter. Mon Not R Astron Soc 427:327. https://doi.org/10.1111/j.1365-2966.2012.21824.x. arXiv:1202.5559 [astro-ph.CO]

Tully RB, Kourkchi E, Courtois HM et al (2023) Cosmicflows-4. Astrophys J 944(1):94. https://doi.org/10.3847/1538-4357/ac94d8. arXiv:2209.11238 [astro-ph.CO]

Turner RJ, Blake C, Ruggeri R (2023) A local measurement of the growth rate from peculiar velocities and galaxy clustering correlations in the 6dF Galaxy Survey. Mon Not R Astron Soc 518(2):2436–2452. https://doi.org/10.1093/mnras/stac3256. arXiv:2207.03707 [astro-ph.CO]

Vanderveld RA, Mortonson MJ, Hu W et al (2012) Testing dark energy paradigms with weak gravitational lensing. Phys Rev D 85:103518. https://doi.org/10.1103/PhysRevD.85.103518. arXiv:1203.3195 [astro-ph.CO]

Wang LM, Steinhardt PJ (1998) Cluster abundance constraints on quintessence models. Astrophys J 508:483–490. https://doi.org/10.1086/306436. arXiv:astro-ph/9804015

Wang S, Hui L, May M et al (2007) Is modified gravity required by observations? An empirical consistency test of dark energy models. Phys Rev D 76:063503. https://doi.org/10.1103/PhysRevD.76.063503. arXiv:0705.0165 [astro-ph]

Weinberg DH, Mortonson MJ, Eisenstein DJ et al (2013) Observational probes of cosmic acceleration. Phys Rept 530:87–255. https://doi.org/10.1016/j.physrep.2013.05.001. arXiv:1201.2434 [astro-ph.CO]

White M et al (2022) Cosmological constraints from the tomographic cross-correlation of DESI luminous red galaxies and planck CMB lensing. JCAP 02(02):007. https://doi.org/10.1088/1475-7516/2022/02/007. arXiv:2111.09898 [astro-ph.CO]

Wilson MJ, White M (2019) Cosmology with dropout selection: straw-man surveys & CMB lensing. JCAP 10:015. https://doi.org/10.1088/1475-7516/2019/10/015. arXiv:1904.13378 [astro-ph.CO]

Winther HA et al (2015) Modified gravity N-body code comparison project. Mon Not R Astron Soc 454 (4):4208–4234. https://doi.org/10.1093/mnras/stv2253. arXiv:1506.06384 [astro-ph.CO]

Yoo J (2010) General relativistic description of the observed galaxy power spectrum: Do we understand what we measure? Phys Rev D 82:083508. https://doi.org/10.1103/PhysRevD.82.083508. arXiv:1009.3021 [astro-ph.CO]

Yoo J, Fitzpatrick AL, Zaldarriaga M (2009) A new perspective on galaxy clustering as a cosmological probe: general relativistic effects. Phys Rev D 80:083514. https://doi.org/10.1103/PhysRevD.80.083514. arXiv:0907.0707 [astro-ph.CO]

Zentner AR (2007) The excursion set theory of halo mass functions, halo clustering, and halo growth. Int J Mod Phys D 16:763–816. https://doi.org/10.1142/S0218271807010511. arXiv:astro-ph/0611454

Zhang J, Hui L, Stebbins A (2005) Isolating geometry in weak lensing measurements. Astrophys J 635:806–820. https://doi.org/10.1086/497676. arXiv:astro-ph/0312348

Zhang P, Liguori M, Bean R et al (2007) Probing gravity at cosmological scales by measurements which test the relationship between gravitational lensing and matter overdensity. Phys Rev Lett 99:141302. https://doi.org/10.1103/PhysRevLett.99.141302. arXiv:0704.1932 [astro-ph]

Zhao GB, Pogosian L, Silvestri A et al (2009) Cosmological tests of general relativity with future tomographic surveys. Phys Rev Lett 103:241301. https://doi.org/10.1103/PhysRevLett.103.241301. arXiv:0905.1326 [astro-ph.CO]

Zhao GB, Pogosian L, Silvestri A et al (2009) Searching for modified growth patterns with tomographic surveys. Phys Rev D 79:083513. https://doi.org/10.1103/PhysRevD.79.083513. arXiv:0809.3791 [astro-ph]

Zhao GB, Giannantonio T, Pogosian L et al (2010) Probing modifications of general relativity using current cosmological observations. Phys Rev D 81:103510. https://doi.org/10.1103/PhysRevD.81.103510. arXiv:1003.0001 [astro-ph.CO]

Zhao GB, Li B, Koyama K (2011) N-body simulations for $f(R)$ gravity using a self-adaptive particle-mesh code. Phys Rev D 83:044007. https://doi.org/10.1103/PhysRevD.83.044007. arXiv:1011.1257 [astro-ph.CO]